





Research Article

Emodin, Physcion, and Crude Extract of *Rhamnus sphaerosperma* var. *pubescens* Induce Mixed Cell Death, Increase in Oxidative Stress, DNA Damage, and Inhibition of AKT in Cervical and Oral Squamous Carcinoma Cell Lines

Thais Fernanda Moreira ¹, Juliana Maria Sorbo,¹ Felipe de Oliveira Souza,¹ Barbara Colatto Fernandes,¹ Fernanda Maria Marins Ocampos,² Daniella Maria Soares de Oliveira,² Carlos Alberto Arcaro ¹, Renata Pires Assis,¹ Andersson Barison,³ Obdulio Gomes Miguel,² Amanda Martins Baviera ¹, Christiane Pienna Soares,¹ and Iguatemy Lourenço Brunetti ¹

¹Department of Clinical Analysis, School of Pharmaceutical Sciences, São Paulo State University (UNESP), 14800-903 Araraquara, SP, Brazil

²Department of Pharmacy, Federal University of Paraná (UFPR), 80210-170 Curitiba, PR, Brazil

³Department of Chemistry, Federal University of Paraná (UFPR), 80210-170 Curitiba, PR, Brazil

Correspondence should be addressed to Iguatemy Lourenço Brunetti; brunetti@fcar.unesp.br

Received 7 March 2018; Revised 8 May 2018; Accepted 20 May 2018; Published 3 July 2018

Academic Editor: Angel Catalá

Copyright © 2018 Thais Fernanda Moreira et al. This is an open access article distributed under the Creative Commons Attribution License, which permits unrestricted use, distribution, and reproduction in any medium, provided the original work is properly cited.

There have been few studies on the pharmacological properties of *Rhamnus sphaerosperma* var. *pubescens*, a native Brazilian species popularly known as “fruto-de-pombo.” The aim of this study was to investigate the scavenging capacity of emodin, physcion, and the ethanolic crude extract of *Rhamnus sphaerosperma* var. *pubescens* against reactive oxygen and nitrogen species, as well as their role and plausible mechanisms in prompting cell death and changes in AKT phosphorylation after cervical (SiHa and C33A) and oral (HSC-3) squamous cell carcinoma treatments. Emodin was shown to be the best scavenger of NO^\bullet and $\text{O}_2^{\bullet-}$, while all samples were equally effective in HOCl/OCl^- capture. Emodin, physcion, and the ethanolic extract all exhibited cytotoxic effects on SiHa, C33A, HSC-3, and HaCaT (immortalized human keratinocytes, nontumorigenic cell line), involving mixed cell death (apoptosis and necrosis) independent of the caspase activation pathway. Emodin, physcion, and the ethanolic extract increased intracellular oxidative stress and DNA damage. Emodin decreased the activation of AKT in all tumor cells, physcion in HSC-3 and HaCaT cells, and the ethanolic extract in C33A and HaCaT cells, respectively. The induction of cancer cell death by emodin, physcion, and the ethanolic crude extract of *Rhamnus sphaerosperma* var. *pubescens* was related to an increase in intracellular oxidative stress and DNA damage and a decrease in AKT activation. These molecules are therefore emerging as interesting candidates for further study as novel options to treat cervical and oral carcinomas.

1. Introduction

Cancer is a major global health concern. High morbidity and mortality rates indicate an increase in the global incidence of cancer, mainly owing to aging populations. Cervical cancer

is the fourth most common cancer diagnosed in women worldwide; it is associated with human papillomavirus (HPV) infection. Despite vaccination efforts against HPV infections, since vaccines may provide cross-protection against some HPV strains known to cause cervical cancer, a

considerable number of female deaths is still attributed to cervical cancer [1].

HPV has often been associated with oncogenesis, since it causes genetic and metabolic changes that favor tumor development. Its targets are p53, retinoblastoma protein (pRb), and the PI3K/AKT pathway. Thus, in addition to cervical cancer, HPV is associated with the induction of other types of cancer, including squamous cell carcinoma of the esophagus and oral cavity (oropharynx, tonsils, and tongue) [1–4].

The PI3K/AKT signaling pathway is important in regulating normal cell processes, such as proliferation, motility, survival, and cell death. Deregulation of this pathway contributes to tumorigenesis in many cancers, including the squamous cell carcinomas. Alterations in AKT, PIK3CA (which encodes for the p110 α catalytic subunit of PI3K), and PTEN have been described in squamous cell carcinomas of oral origin (HSC-2, HSC-3, and HSC-4), as well as in cell carcinomas of cervical origin (HeLa, CaSki, SiHa, and C33A) [5–8].

Hyperactivation of the PI3K/AKT pathway in tumor cells leads to a continuous flow of substrates through the glycolytic pathway, contributing with the Warburg effect, (increased glucose uptake and lactate production, even in the presence of oxygen and mitochondrial metabolism) which is highly dependent on complete AKT activation. Complete activation of AKT requires PI3K activity and phosphorylation of both the Thr-308 residue by PDK-1 and the Ser-473 residue by mTORC2. In contrast, PTEN acts as a tumor suppressor and plays an essential role in inhibiting PI3K/AKT signaling [9–12]. AKT regulates the cell cycle and proliferation directly by acting on CDKI (kinase-dependent cyclin inhibitors), such as p21 and p27, and indirectly by modulating the levels of cyclin D1 and p53. AKT also promotes the phosphorylation and inactivation of transcriptional factors FOXO (Forkhead box O); FOXO factors act directly on the cell cycle, DNA repair, and apoptosis, and their inactivation promotes a decrease in the expression of negative regulators of the cell cycle, such as the proteins related to retinoblastoma, p130, CDKI, and p27 [13].

In the metabolic state of neoplastic cells, RONS, such as superoxide anion ($O_2^{\bullet-}$), hydrogen peroxide (H_2O_2), and nitric oxide ($^{\bullet}NO$), occur abundantly. The effects of RONS can vary depending on their concentrations in the cells. Intracellular nitric oxide ($^{\bullet}NO$) causes inactivation of PTEN through S-nitrosylation and consequently ubiquitin-mediated proteasomal degradation. Changes in the PTEN status are associated with the redox status and are important for cell survival and proliferation [14]. In these cells, RONS levels are controlled via antioxidant defenses. An increase in NADPH production by glutamine metabolism and the pentose phosphate pathway facilitate glutathione (GSH) regeneration as well as the expression of enzymes that act on RONS metabolism, such as catalase, SOD, NOX-1, and DUOX-POD [15–17].

Inhibition of the PI3K/AKT pathway culminates in the loss of regulation of mechanisms involved in tumor cell proliferation and survival, thus emerging as an important therapeutic target for tumor suppression. Compounds able to unbalance the redox state and to promote alterations in

the PI3K/AKT pathway may be useful to induce cell death in tumor cells.

Anti-inflammatory, antioxidant, antihypertensive, anti-mutagenic, and apoptosis-inducing properties have been described for species of the genus *Rhamnus* [18–20]. In our previous study, chrysophanol and physcion (anthraquinones) and stigmasterol and sitosterol (phytosterols) were isolated from the ethanolic extract of *R. sphaerosperma* var. *pubescens* stems; the extract and its fractions exhibited antioxidant properties and the ability to inhibit liporoxidation [21].

Anthraquinones have a chemical structure similar to that of anthracyclines, a class of chemotherapeutic agents such as doxorubicin, which demonstrate effectiveness in several tumor types [22]. These chemical properties of anthraquinones, combined with molecular modeling and other tools, together contribute to the improvement of the therapeutic arsenal against squamous cell carcinoma. From this perspective, the present study identified different responses of the anthraquinones emodin and physcion and crude extracts from *Rhamnus sphaerosperma* var. *pubescens* related to the ability to capture reactive oxygen and nitrogen species. Furthermore, the mechanisms of cell death induction and the changes in AKT phosphorylation levels were analyzed after treatments with emodin, physcion, or ethanolic crude extract of *Rhamnus sphaerosperma* var. *pubescens*, in the following cancer cell lines: SiHa, C33A (cervical squamous cell carcinomas), and HSC-3 (oral squamous cell carcinomas).

2. Materials and Methods

2.1. Equipment and Chemicals. NMR spectra were recorded on a Bruker Avance III 600 $^{\circ}$ (Bruker, Massachusetts, USA). The capture assays were performed in a microplate spectrophotometer (PowerWave XS2, BIOTEK $^{\circ}$, Vermont, USA). Fetal bovine serum was purchased from Cultilab $^{\circ}$, São Paulo, Brazil. Fluorescein diacetate, propidium iodide, and Hoechst 33342 were purchased from Invitrogen $^{\circ}$, Ontario, Canada. Annexin-V conjugated with FITC was purchased from Life Technologies $^{\circ}$, Ontario, Canada. Sodium pyrophosphate, sodium fluoride, and sodium nitroprusside were purchased from Merck $^{\circ}$, Darmstadt, Germany. The TBARS assay was performed in a microplate spectrofluorimeter (Synergy 5, BIOTEK, Vermont, USA). The comet assay was performed in fluorescence microscope (ECLIPSE 50i; Nikon Instruments Inc., Nikon do Brasil LTDA., São Paulo, Brazil) coupled with a photograph camera (DS-Ri1; Nikon Instruments Inc., Nikon do Brasil LTDA., São Paulo, Brazil). Western blot analysis was performed in a Bio-Rad miniature gel apparatus and miniature transfer apparatus (Mini-Protean, Bio-Rad Laboratories, California, EUA), and a C-Digit $^{\circ}$ Blot Scanner (LI-COR, Nebraska, USA) was used to capture chemiluminescent signals in membranes.

Ultrapure water was used in all assays was obtained in a Milli-Q $^{\circ}$ Millipore System, USA.

Deuterated solvent chloroform ($CDCl_3$) was purchased from Cambridge Isotope Laboratories (Massachusetts, USA). Dimethyl sulfoxide (DMSO, 99.9%, v/v), trolox, gallic acid, quercetin, curcumin, ascorbic acid, catalase, doxorubicin, Dulbecco's modified Eagle medium, Ham F10 and F12

nutrient mixtures, hydrocortisone penicillin and streptomycin solution, sodium bicarbonate, kanamycin, fluorogenic substrate for caspase-3 (Ac-Asp-Met-Gln-Asp-AMC), fluorescein isothiocyanate, dithiothreitol, Tris, sodium dodecyl sulfate, β -mercaptoethanol, aprotinin, PMSF, leupeptin, sodium orthovanadate, NaOCl, 3,3',5,5'-tetramethylbenzidine, potassium iodide, NADH, phenazinemetasulfate, nitroblue tetrazolium, sulfanilic acid, N-(1-naphthalenediamine), cytochalasin B, and trypsin were purchased from Sigma-Aldrich® (Sigma-Aldrich Brasil Ltda., São Paulo, Brazil). Fetal bovine serum (Cultilab®, São Paulo, Brazil), fluorescein diacetate, propidium iodide and Hoechst 33342 (Invitrogen®, Ontario, Canada), and annexin-V conjugated with FITC (Life Technologies®, Ontario, Canada). Sodium pyrophosphate, sodium fluoride, and sodium nitroprusside (Merck®, Darmstadt, Germany).

Antibodies anti-AKT, anti-p-[Ser-473]-AKT, anticaspase-3, anti-BAX, anti-BCL-2, and anti-rabbit IgG conjugated with horseradish peroxidase were purchased from Cell Signaling Technology® (Massachusetts, USA), and anti-GAPDH was purchased from CUSABIO Technology LLC® (Texas, USA).

2.2. Plant Material Isolation and Identification. The plant species were collected at the Federal University of Paraná, Curitiba, Paraná, Brazil (25°26'52"S 49°14'21"W), during the morning hours of May 2011 and July 2013. Botanical identification was carried out at the Municipal Botanical Museum of Curitiba (Paraná, Brazil).

Dry and powdered stems of *Rhamnus sphaerosperma* var. *pubescens* were subjected to extraction with absolute ethanol, and the ethanolic crude extract (EERs) was separated into a liquid-liquid partition with hexane (hexane fraction—HFRs), chloroform (chloroform fraction—CFRs), and ethyl acetate (ethyl acetate fraction—EAFRs). Both methods were performed in Soxhlet equipment at 60°C. The hexane fraction was subjected to column chromatography using silica gel 60 and a mobile phase composed of hexane and ethyl acetate, and ethyl acetate and methanol, with gradients of increasing polarities (starting from 100% *v/v* hexane to 100% *v/v* ethyl acetate and from 100% *v/v* ethyl acetate to 80% *v/v* methanol).

2.3. RONS Capture Assays

2.3.1. $O_2^{\bullet-}$ Capture Assay. This method is based on the *in vitro* formation of $O_2^{\bullet-}$ via nonenzymatic reactions between reduced nicotinamide adenine dinucleotide (NADH), phenazinemetasulfate (PMS), and oxygen dissolved in the medium. The reactive species formed promotes the reduction of nitroblue tetrazolium (NBT), generating a formazane salt, which is quantified by spectrophotometry (560 nm). The assay was performed in sodium pyrophosphate buffer (25 mM, pH 8.3), with PMS (0.372 mM), NBT (0.6 mM), NADH (1.56 mM), and various concentrations of the samples, with a final reaction volume of 300 μ L. After incubation in the dark at room temperature for 7 min, the absorbance was measured at 560 nm [23].

2.3.2. HOCl/OCl⁻ Capture Assay. HOCl/OCl⁻ has the ability to oxidize 3,3',5,5'-tetramethylbenzidine (TMB), generating a blue staining compound detected at 652 nm. Initially, the OCl⁻ concentration was determined by its molar extinction coefficient ($\epsilon = 350 \text{ M}^{-1} \cdot \text{cm}^{-1}$ at 292 nm) [24]. The TMB solution (2.8 mM) was prepared from its dissolution in dimethylformamide (50%, *v/v*), 0.8 M acetic acid (49%, *v/v*), and 0.01 M potassium iodide (1%, *v/v*). The reaction began with incubation of the samples at different concentrations, diluted in sodium phosphate buffer (50 mM, pH 7.4) with HOCl/OCl⁻ (30 μ M), and revealed with TMB (2.8 mM) at a final reaction volume of 300 μ L [25–27].

2.3.3. *NO Capture Assay. Nitric oxide, generated from the dissolution of sodium nitroprusside in an aqueous solution with pH 7.4, reacts with oxygen in the medium, generating nitrate and nitrite. The concentration of nitrite is determined spectrophotometrically, by subjecting it to reaction with Griess reagent: 1.0% (*w/v*) sulfanilic acid, 0.1% (*w/v*) N-(1-naphthalenediamine), and 2.5% (*v/v*) phosphoric acid, at 540 nm. The samples were incubated at different concentrations with sodium nitroprusside (4 mM) in a sodium phosphate buffer (20 mM, pH 7.4) for 150 min at room temperature. Then Griess reagent was added, and at a final reaction volume of 300 μ L, the absorbance was measured at 540 nm [28].

2.4. Assays for Cell Death

2.4.1. Cell Culture. Cell lines SiHa (ATCC® HTB35™), C33A (ATCC HTB31™), and HaCaT (CLS 300493) were grown in DMEM (Dulbecco's modified Eagle medium) with Ham F10 (F10 Ham nutrient mixture). The HSC-3 cell line (JCRB: JCR 0623) was grown in DMEM with Ham F12 (F12 Ham nutrient mixture), hydrocortisone (0.4 μ g/L), and ascorbic acid (50 mg/L). All media were supplemented with fetal bovine serum (10% *v/v*), penicillin (100 U/mL), streptomycin (100 μ g/mL), amphotericin B (0.25 mg/L), kanamycin (0.1 g/L), and HEPES (5.96 g/L). Cultures were grown in a sterile atmosphere at 37°C under 5% CO₂.

Emodin, physcion, ethanolic extract, and hexane fraction from *Rhamnus sphaerosperma* var. *pubescens* stems were used to study cell death mechanisms. The working concentrations were established by a sulforhodamine B assay (data not shown). Chrysophanol did not induce cytotoxicity for all cell lines studied.

2.4.2. Cytomorphological Viability Assay with Hoechst 33342, Propidium Iodide, and Fluorescein Diacetate. The cells were plated (5×10^3 cells/well) in 96-well plates for 24 h, and the treatments were performed for 12 h or 24 h. After the treatment periods, the plate was centrifuged at 1258g, and each well was washed with phosphate buffered saline (PBS) and centrifuged again under the same conditions. The distinction between viable cells and dead cells in apoptosis and necrosis was performed by adding a solution (100 μ L/well) containing fluorescein diacetate (3.5 μ g/mL), propidium iodide (2.5 μ g/mL), and Hoechst 33342 (1.5 μ g/mL) in PBS. After incubation for 10 min at room temperature in the dark,

the images were acquired and analyzed using an imaging cytometer IN Cell Analyzer 2000 [29].

2.4.3. Annexin-V Cell Death Assay. The cells were plated (5×10^3 cells/well) in 96-well plates for 24 h, and the treatments were performed for 12 h or 24 h. After the treatment period, the plate was centrifuged at 1258g, and each well was washed with PBS and centrifuged again under the same conditions. After washing, 100 μ L/well of annexin-V binding buffer (10 mM HEPES, 140 mM NaCl, and 2.5 M CaCl_2) containing annexin-V/FITC (1.3 μ g/mL) and Hoechst 33342 (1.6 μ g/mL) was added, followed by incubation for 15 minutes at 4°C in darkness. After incubation, 20 μ L/well of propidium iodide (1 μ g/mL, diluted in the buffer described above) was added. The images were acquired and analyzed using an imaging cytometer IN Cell Analyzer 2000 [30].

2.4.4. Caspase-3 Activity Assay. The cells were plated (1×10^4 cells/well) in 96-well plates for 24 h, and the treatments were performed for 6 h. After the treatment period, the plate was centrifuged at 1258 \times g, and each well was washed with PBS and centrifuged again under the same conditions. After washing, the cells were permeabilized with a 0.5% (w/v) saponin solution (dissolved in culture medium containing 5 mM DTT and 2 mM EDTA) for 10 min. After the permeabilization step, a solution with caspase-3-specific fluorogenic substrate (20 μ M) and propidium iodide (2.5 μ g/mL—for nuclear staining) was added (100 μ L/well). The images were immediately acquired and analyzed using an imaging cytometer IN Cell Analyzer 2000 [31].

2.4.5. Western Blot Analysis. The cells were plated (8×10^5 cells/well) in 6-well plates for 24 h, and the treatments were performed for 24 h. After the treatment period, the cells were washed with PBS and lysed with lysis solution containing Tris (125 mM, pH 6.8), sodium dodecyl sulfate (10%, w/v), β -mercaptoethanol (1%, v/v), protease inhibitors (5 μ g/mL aprotinin, 1 mM PMSF, and 2.34 mM leupeptin), and phosphatase inhibitors (10 mM sodium pyrophosphate, 100 mM sodium fluoride, and 10 mM sodium orthovanadate). After lysis, the cell lysates were heated to 95°C for 8 min, and the samples were stored at -80°C until use; an aliquot was separated for quantification of total proteins by the Lowry method [32].

Proteins from cell lysates were separated by 10% (w/v) SDS polyacrylamide gel electrophoresis (SDS-PAGE) [33]. Proteins were transferred to nitrocellulose membranes (Amersham™ Protran™—GE Health Care) [34] and blocked for 1 hour at room temperature with 10% (w/v) nonfat dried milk in Tris-buffered saline with Tween 20 (10 mM Tris, 125 mM NaCl, and 0.1% v/v Tween 20). The membranes were then incubated overnight at 4°C with specific primary antibodies: anti-AKT (1:500), anti-p-[Ser-473]-AKT (1:500), anticaspase-3 (1:1000), anti-BAX (1:1000), anti-BCL-2 (1:1000), and anti-GAPDH (1:1000). After washing with Tris-buffered saline and Tween 20, the membranes were incubated with secondary antibodies (HRP-conjugated anti-rabbit IgG, 1:1000) for one hour at room temperature. After washing, the membranes were revealed using a chemiluminescent

substrate (5 mM luminol, 8 mM hydrogen peroxide, 4 mM p-iodophenylboronic acid, and 0.1 M Tris-HCl; pH 8.8) [35]. Chemiluminescent bands were captured with a C-Digit Blot Scanner (LI-COR, Lincoln, NE), and the band intensities were analyzed using LI-COR Image Studio 4.0.

2.5. Oxidative Damage Analysis

2.5.1. TBARS Assay. The cells were plated (2×10^5 cells/well) in 24-well plates for 24 h, and the treatments were performed for 24 h. After the treatment, the culture medium of each well (200 μ L) was used to quantify TBARS via reaction with 800 μ L of an aqueous mixture of thiobarbituric acid (0.8%, w/v) diluted with acetic acid (20%, v/v) and sodium dodecyl sulfate (8.1%, w/v). The tubes were incubated at 95°C for 60 min, and the fluorescence intensity was measured with excitation and emission wavelengths of 510 and 553 nm, respectively, using 1,1,3,3-tetramethoxypropane as a standard. The results were expressed as μ M of TBARS [36].

2.6. DNA Damage Analysis

2.6.1. Micronuclei Assay. The cells were plated (4×10^3 cells/well) in 96-well plates for 24 h, and the treatments were performed for 24 h. After treatment, the wells were washed with PBS and incubated with cytochalasin B (6 μ g/mL) for 36 h at 37°C to block cytokinesis, allowing observation of multinucleated cells. Thereafter, the cells were fixed with absolute ethanol for 30 minutes and stained with fluorescein isothiocyanate (FITC) (1 μ g/mL) for 1 h for cytoplasmic staining and with Hoechst 33342 (10 μ g/mL) for 30 min for DNA staining. The images were acquired and analyzed using the imaging cytometer IN Cell Analyzer 2000 [37].

2.6.2. Comet Assay. The cells were plated (1×10^5 cells/well) in 24-well plates for 24 h, and the treatments were performed for 6 h. The comet assay was performed as described by Singh et al. [38] and Tice et al. [39]. For each test (samples and respective concentrations), 50 cells were analyzed using TriTek Comet Score TM version 1.5 software. The percentage of DNA in the tail was used to analyze the amount of fragmented DNA [40].

2.7. Statistical Analysis. For cell death and caspase activity assays, one-way analysis of variance (ANOVA) followed by the Tukey's post-test was applied. For the micronuclei, TBARS, and Western blot assays, ANOVA followed by the Newman-Keuls post-test was applied. For the comet assay, a Kruskal-Wallis test with a Dunn's post-test was applied. GraphPad Prism 6.0 software was used in these analyses.

3. Results and Discussion

3.1. Chrysophanol, Emodin, and Physcion Were Isolated from *R. sphaerosperma* var. *pubescens*. The crude ethanolic extract of *R. sphaerosperma* and its fractions underwent hydrogen magnetic resonance analysis (^1H NMR). The ^1H NMR spectra showed peaks corresponding to anthraquinone nuclei, except in the ethyl acetate fraction. Characterization of the anthraquinone nucleus by ^1H NMR is defined by chemical shifts in the region of 10–12 ppm of the spectrum, corresponding to

TABLE 1: Chemical shift values and coupling constants of ^1H NMR spectra for chrysophanol, emodin, and physcion.

Position	Chrysophanol	Chemical shift (ppm) ^1H Emodin	Physcion
1 (C)–OH	12.09	12.21 (s)	12.10 (s)
2 (CH)	7.09 (m)	7.08 (dq; $J = 1.6 \text{ Hz} \text{ e } 0.8 \text{ Hz}$)	7.07 (m)
3 (methyl)	2.46 (s)	2.45 (dd; $J = 0.8 \text{ Hz} \text{ e } 0.5 \text{ Hz}$)	2.45 (s)
4 (CH)	7.65 (m)	7.60 (dq; $J = 1.6 \text{ Hz} \text{ e } 0.5 \text{ Hz}$)	7.62 (m)
5 (CH)	7.81 (d; $J = 7.8 \text{ Hz}$)	7.23 (d; $J = 2.41 \text{ Hz}$)	7.35 (d; $J = 2.61 \text{ Hz}$)
6 (CH)	7.68 (dd; $J = 8.5 \text{ Hz} \text{ e } 7.8 \text{ Hz}$)	—	—
6 (methoxyl)	—	—	3.93 (s)
7 (CH)	7.28 (d; $J = 8.5 \text{ Hz}$)	6.63 (d; $J = 2.4 \text{ Hz}$)	6.67 (d; $J = 2.60 \text{ Hz}$)
8 (C)–OH	12.11 (s)	12.31 (s)	12.29 (s)

J = coupling constant; d = doublet; dd = double doublet; dq = double quartet; s = singlet; t = triplet; m = multiplet.

hydroxyl groups chelated by hydrogen bonds, and chemical shifts between 6 and 7 ppm, characteristic of ortho- and metacoupling of hydrogen [41]. After column chromatography of the hexane fraction, three crystalline samples were isolated and identified with ^1H NMR as chrysophanol (1,8-dihydroxy-3-methylanthraquinone), physcion (1,8-dihydroxy-6-methoxy-3-methylanthraquinone), and emodin (1,6,8-trihydroxy-3-methylanthraquinone). The chemical shift and coupling constant values of the ^1H NMR spectra for the anthraquinones are shown in Table 1.

To the best of our knowledge, the present study is the first to isolate these compounds in *R. sphaerosperma* var. *pubescens*. However, they are very common in other species of the genus *Rhamnus* (e.g., *Rhamnus frangula*), in addition to several other plant and animal species, as well as microorganisms (fungi, bacteria, and lichens) and insects [41].

3.2. Samples from *R. sphaerosperma* var. *pubescens* Exhibited Capture Capacity for $\text{O}_2^{\bullet-}$, HOCl/OCl^- , and $\bullet\text{NO}$. The effective concentration that promotes 50% inhibition (EC_{50}) in the capture of the reactive species was calculated by linear regression. These values for samples and standards were statistically compared for each test, with lower EC_{50} values indicating greater effectiveness. These results are presented in Table 2. Curcumin (β -diketone) and quercetin (flavonoid) showed higher efficiency for all reactive species studied. Gallic acid (phenolic acid) showed lower efficiency against $\bullet\text{NO}$, and Trolox (tocopherol's water-soluble analog) showed higher EC_{50} (lower efficiency) in the capture of HOCl/OCl^- and $\text{O}_2^{\bullet-}$, and there is no activity on $\bullet\text{NO}$ (Table 2).

Among all compounds used as controls in assays to assess RONS capture capacity, curcumin is the most well known for its cytotoxic capacity. It has been shown to be effective in the induction of cell death in various tumor cell lines [42]; therefore, it was also used as a control in the cell death assays.

RONS capture capacity has been reported for several biomolecules, since RONS are determinants of metabolic and proliferative controls, most notably in tumor cells [43].

Oncogenic transformation is functionally associated with the expression of cell membrane enzymes, such as NOX1, which generates $\text{O}_2^{\bullet-}$ that undergoes spontaneous or catalyzed (by SOD) dismutation to H_2O_2 , which is decomposed into H_2O and O_2 by the action of catalase; the conversion

TABLE 2: Capture capacity for $\text{O}_2^{\bullet-}$, HOCl/OCl^- , and $\bullet\text{NO}$.

	EC_{50} ($\mu\text{g}/\text{mL}$)		
	$\text{O}_2^{\bullet-}$	HOCl/OCl^-	$\bullet\text{NO}$
Curcumin	$59.45 \pm 5.85 \text{ b}$	$0.5336 \pm 0.081 \text{ b}$	$15.69 \pm 1.03 \text{ b}$
Gallic acid	$18.81 \pm 0.46 \text{ c}$	$0.2843 \pm 0.02 \text{ b}$	$604.5 \pm 52.52 \text{ a}$
Quercetin	$13.48 \pm 0.23 \text{ c}$	$0.2594 \pm 0.04 \text{ b}$	$4.411 \pm 1.69 \text{ c}$
Trolox	$436.6 \pm 9.39 \text{ a}$	$4.578 \pm 0.14 \text{ a}$	—
EERs	$100.5 \pm 0.68 \text{ d}$	$3.195 \pm 0.09 \text{ c}$	$95.43 \pm 8.73 \text{ d}$
HFRs	$409.5 \pm 26.36 \text{ a}$	$4.99 \pm 0.15 \text{ a}$	$152.5 \pm 4.11 \text{ e}$
CFRs	$348.7 \pm 12.02 \text{ e}$	$3.028 \pm 0.25 \text{ c}$	$148.2 \pm 10.34 \text{ e}$
EAFRs	$144.7 \pm 10.67 \text{ d}$	$2.323 \pm 0.12 \text{ d}$	$49.7 \pm 13.79 \text{ f}$

	EC_{50} (μM)		
	$\text{O}_2^{\bullet-}$	HOCl/OCl^-	$\bullet\text{NO}$
Curcumin	$112.9 \pm 11.14 \text{ b}$	$1.014 \pm 0.15 \text{ b}$	$30.62 \pm 2.01 \text{ b}$
Gallic acid	$110.6 \pm 2.72 \text{ b}$	$1.672 \pm 0.10 \text{ b}$	$3556 \pm 309 \text{ a}$
Quercetin	$44.61 \pm 0.75 \text{ c}$	$0.8583 \pm 0.14 \text{ b}$	$14.59 \pm 5.58 \text{ b}$
Trolox	$1813 \pm 52.81 \text{ a}$	$17.82 \pm 0.55 \text{ a}$	—
Emodin	$140.8 \pm 1.44 \text{ d}$	$26.56 \pm 0.74 \text{ c}$	$52.03 \pm 4.28 \text{ c}$
Physcion	—	$33.1 \pm 4.06 \text{ c}$	$377 \pm 16.71 \text{ d}$
Chrysophanol	—	$23.56 \pm 1.12 \text{ c}$	$243 \pm 18.3 \text{ e}$

Results are expressed as mean of the $\text{EC}_{50} \pm$ standard error ($M \pm \text{SE}$), analyzed by one-way ANOVA with Tukey's post-test (different letters represent statistical difference) (— = no activity).

of H_2O_2 into HOCl occurs by the action of free peroxidase released by DUOX-POD, in the presence of chloride. This module of NOX1/SOD/catalase/DUOX-POD enzymes has been found in bona fide tumor cells derived from different tissues. Selective signaling for apoptosis in transformed cells has been reported in dominant pathways, such as those signaled by HOCl/OCl^- and $\bullet\text{NO}/\text{ONOO}^-$, and in less important pathways, such as the nitryl chloride and Fenton/Haber-Weiss reactions. Based on (i) peroxidase action, (ii) the dominant processes that generates peroxynitrite in a reaction between $\bullet\text{NO}$ and $\text{O}_2^{\bullet-}$ and the decomposition of peroxynitrous acid into $\bullet\text{NO}_2$ and $\bullet\text{OH}$, and (iii) the reaction between HOCl and $\text{O}_2^{\bullet-}$ to produce $\bullet\text{OH}$, Cl^- , and O_2 , the $\bullet\text{OH}$ causes lipoperoxidation and triggers the onset of the mitochondrial pathway of apoptosis [44, 45].

The ethyl acetate fraction of *Rhamnus sphaerosperma* var. *pubescens* (EAFRs) was more efficient for HOCl/OCl⁻ and •NO capture, yet both the crude extract (EERs) and EAFRs exhibit similar behavior for the capture of O₂•⁻. These samples are the most effective of those isolated from *R. sphaerosperma* var. *pubescens*. For the ethanolic crude extract and fractions, the presence of anthraquinones in their composition did not influence their capture capacity. EAFRs have no anthraquinones and presented better efficacy when compared to the other fractions that contain anthraquinone compounds, showing equivalency to the crude extract. Thus, it is possible that the capture capacity of the ethanolic crude extract and its fractions is due to the combined effects and/or synergism of compounds not yet identified.

Emodin showed better O₂•⁻ and •NO capture capacity, while other anthraquinones were not active for this species. In the HOCl/OCl⁻ capture assay, there were no statistically significant differences among anthraquinones (Table 2). Few structural differences are observed in these compounds; the presence of an electron-donor group (methoxyl) in the structure of physcion worsens the capture efficiency of the studied reactive species in comparison with an electron-acceptor group (hydroxyl) in the meta position of the emodin structure. The quinone nucleus of the anthraquinones possesses recognized redox capacity, with intermediate formation of the semiquinone radical and subsequent stabilization in hydroquinone [46–48].

Based on these data, we would expect that the treatment of tumor cells with emodin can result in the capture of these reactive species (O₂•⁻ and/or •NO) in the cell environment, causing changes in RONS signaling, which might alter the balance and status of cell survival and proliferation. Additionally, with the formation of semiquinone, toxicity may also occur. The same cannot be attributed to physcion, which was efficient only in capturing HOCl/OCl⁻; nevertheless, it also shows relevant cytotoxicity in cell death assays. Conversely, chrysophanol, which is also efficient in capturing HOCl/OCl⁻, was not able to exert cytotoxicity, suggesting that the semiquinones produced from the interaction of these anthraquinones with cellular RONS have different cytotoxic capacities. However, further experiments are necessary to explore these hypotheses.

3.3. Emodin, Physcion, EERs, and HFRs Induced Mixed Cell Death Independent of Caspase-3 Activation. The cytotoxic profile of *R. sphaerosperma* var. *pubescens* was analyzed against different normal cell lines (HaCaT) or tumor cell lines (SiHa, C33A, and HSC-3) by the sulforhodamine B assay (data not shown). Chrysophanol and the EAFRs did not exert toxic effects on the evaluated cell lines, while emodin, physcion, ethanolic crude extract (EERs), and its hexane fraction (HFRs) showed higher cytotoxic effects; therefore, the latter were selected for additional cell death assays.

Emodin was studied at concentrations from 46.3 to 185.0 μM (12.5 to 50.0 μg/mL), physcion was studied at concentrations from 43.8 to 175.0 μM (12.5 to 50.0 μg/mL), and ethanolic crude extract (EERs) and its hexane fraction (HFRs) were evaluated at concentrations from 25.0 to 100.0 μg/mL.

For the SiHa and C33A cell lines, the time of treatment was 24 h, and for the HSC-3 and HaCaT cell lines, it was 12 h. As positive controls for all cell lines, curcumin induced predominantly apoptosis and doxorubicin induced necrosis.

All tested samples showed a mixed cell death profile for the SiHa cell line, with the presence of cells that were classified as morphologically and biochemically in apoptosis (early or late) and necrosis; emodin was more effective than physcion (Figure 1). For C33A cells, the cytomorphological assay revealed cell death predominantly with necrosis features, while in the annexin-V assay, the presence of apoptosis was observed. All samples were more efficient in the C33A cell line than in SiHa, except for physcion (Figure 2).

In HSC-3 cells, EERs was more effective than HFRs, with mixed cell death. The anthraquinones were less efficient than EERs and HFRs, while emodin and physcion exhibited no differences in this cell line with regard to the induction of mixed cell death (Figure 3). Cell death induced in HaCaT (normal cell line) was mixed, with both apoptosis and necrosis, except for EERs that induced necrosis in all tested concentrations. All samples were more toxic in HaCaT than HSC-3 (tumor cell line), after 12 hours of treatment (Figure 4).

Caspase-3 activity is a hallmark of classical apoptosis. Treatments with anthraquinones, EERs, and HFRs did not promote significant changes in caspase-3 activity (Figure 5); thus, it can be suggested that cell death occurs independently of the caspase-3 pathway and that the morphological and biochemical alterations observed are due to the activation of other biochemical pathways, such as caspase-1 activation, release of interleukins (IL-1β and IL-18), and caspase-7 activation, culminating in an unusual process of cell death in which cells may exhibit morphological characteristics of apoptosis and/or necrosis [49]. In the assay of the present study, only the cells treated with curcumin showed activation of caspase-3; treatment with doxorubicin did not change the caspase-3 activity (Figure 5).

To the best of our knowledge, the present study is the first to describe cell death promoted by complex mixtures of the extract and fractions from *Rhamnus sphaerosperma* var. *pubescens*. However, emodin and physcion have previously been recognized for their promotion of cell death. In lung tumor cells A549, H460, and CH27, 10 μM emodin inhibited cell growth after 48 hours of treatment and 50 μM emodin induced apoptosis with DNA fragmentation. In A549 cells, 50 μM emodin also induced activation of caspases-2, -3, and -9 after 12 h of treatment [50]. Caspase-dependent cell death was also observed in Bu 25TK (cervical cell line) and SMMC-7721 and HepG2 (hepatocellular carcinomas) [51, 52].

Some studies have demonstrated the cytotoxic effects of physcion, dependent on the activation of caspases, and cell cycle arrest in HeLa (cervical cancer cells), SW620 (colorectal cancer cells), and MDA-MB-231 (breast cancer cells) [53–55]. Studies using physcion-8-O-β glucopyranoside have also shown significant cytotoxic activity in HepG2, A549, and HEM (human melanoma cells) [56–58].

Thus, the findings of the present study revealed that emodin and physcion induced mixed cell death, independent of caspases, in cervical cell lines (SiHa and C33A), after 24 h

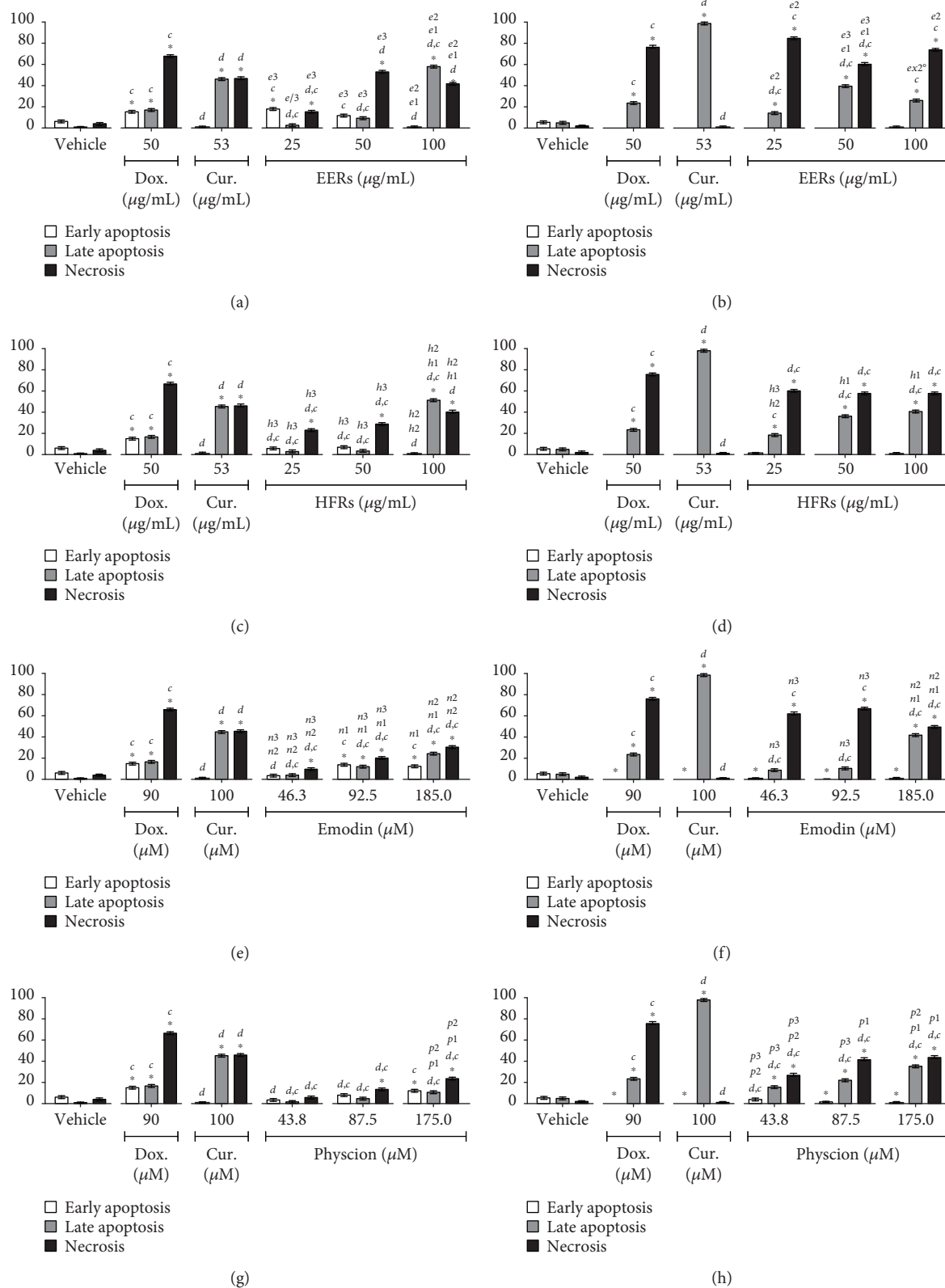


FIGURE 1: Cell death analysis in SiHa cells. Cytomorphological viability assay for (a) EERs, (c) HFRs, (e) emodin, and (g) physcion. Annexin-V assay for (b) EERs, (d) HFRs, (f) emodin, and (h) physcion. Comparison with significant statistical difference between treatments: vehicle (*); doxorubicin (d); curcumin (c); EERs: 25 $\mu\text{g/mL}$ (e1); EERs: 50 $\mu\text{g/mL}$ (e2); EERs: 100 $\mu\text{g/mL}$ (e3); HFRs: 25 $\mu\text{g/mL}$ (h1); HFRs: 50 $\mu\text{g/mL}$ (h2); HFRs: 100 $\mu\text{g/mL}$ (h3); emodin: 46.3 μM (n1); emodin: 92.8 μM (n2); emodin: 185.0 μM (n3); physcion: 43.8 μM (p1); physcion: 87.5 μM (p2); physcion: 175.0 μM (p3); and cell status: early apoptosis, late apoptosis, and necrosis. Results are expressed as mean of three independent experiments \pm standard error ($M \pm SE$), analyzed by one-way ANOVA with Tukey's pos-t-test, $p \leq 0.05$.

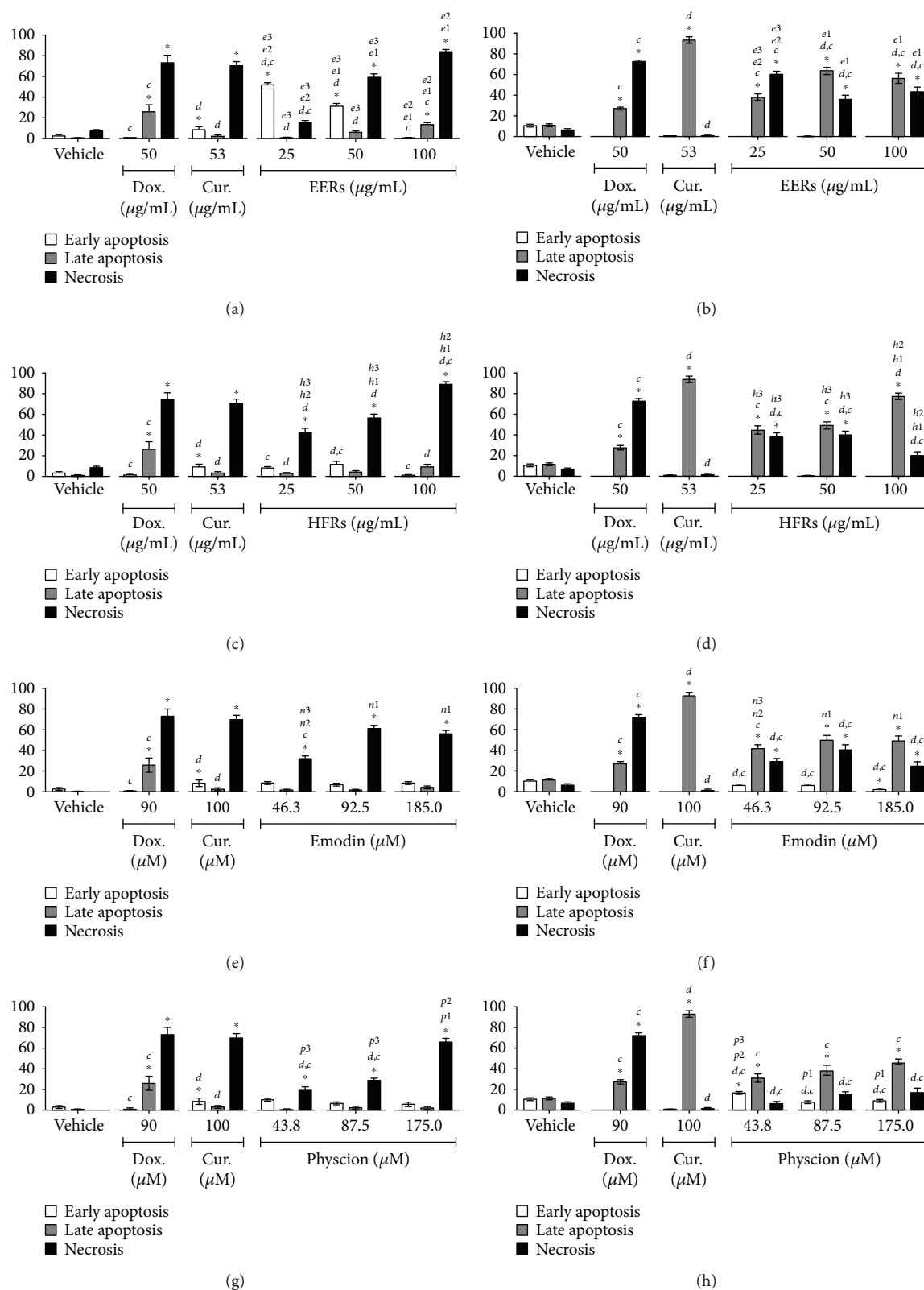


FIGURE 2: Cell death analysis in C33A cells. Cytomorphological viability assay for (a) EERs, (c) HFRs, (e) emodin, and (g) physcion. Annexin-V assay for (b) EERs, (d) HFRs, (f) emodin, and (h) physcion. Comparison with significant statistical difference between treatments: vehicle (*); doxorubicin (d); curcumin (c); EERs: 25 $\mu\text{g/mL}$ (e1); EERs: 50 $\mu\text{g/mL}$ (e2); EERs: 100 $\mu\text{g/mL}$ (e3); HFRs: 25 $\mu\text{g/mL}$ (h1); HFRs: 50 $\mu\text{g/mL}$ (h2); HFRs: 100 $\mu\text{g/mL}$ (h3); emodin: 46.3 μM (n1); emodin: 92.5 μM (n2); emodin: 185.0 μM (n3); physcion: 43.8 μM (p1); physcion: 87.5 μM (p2); physcion: 175.0 μM (p3); and cell status: early apoptosis, late apoptosis, and necrosis. Results are expressed as mean of three independent experiments \pm standard error ($M \pm SE$), analyzed by one-way ANOVA with Tukey's post-test, $p \leq 0.05$.

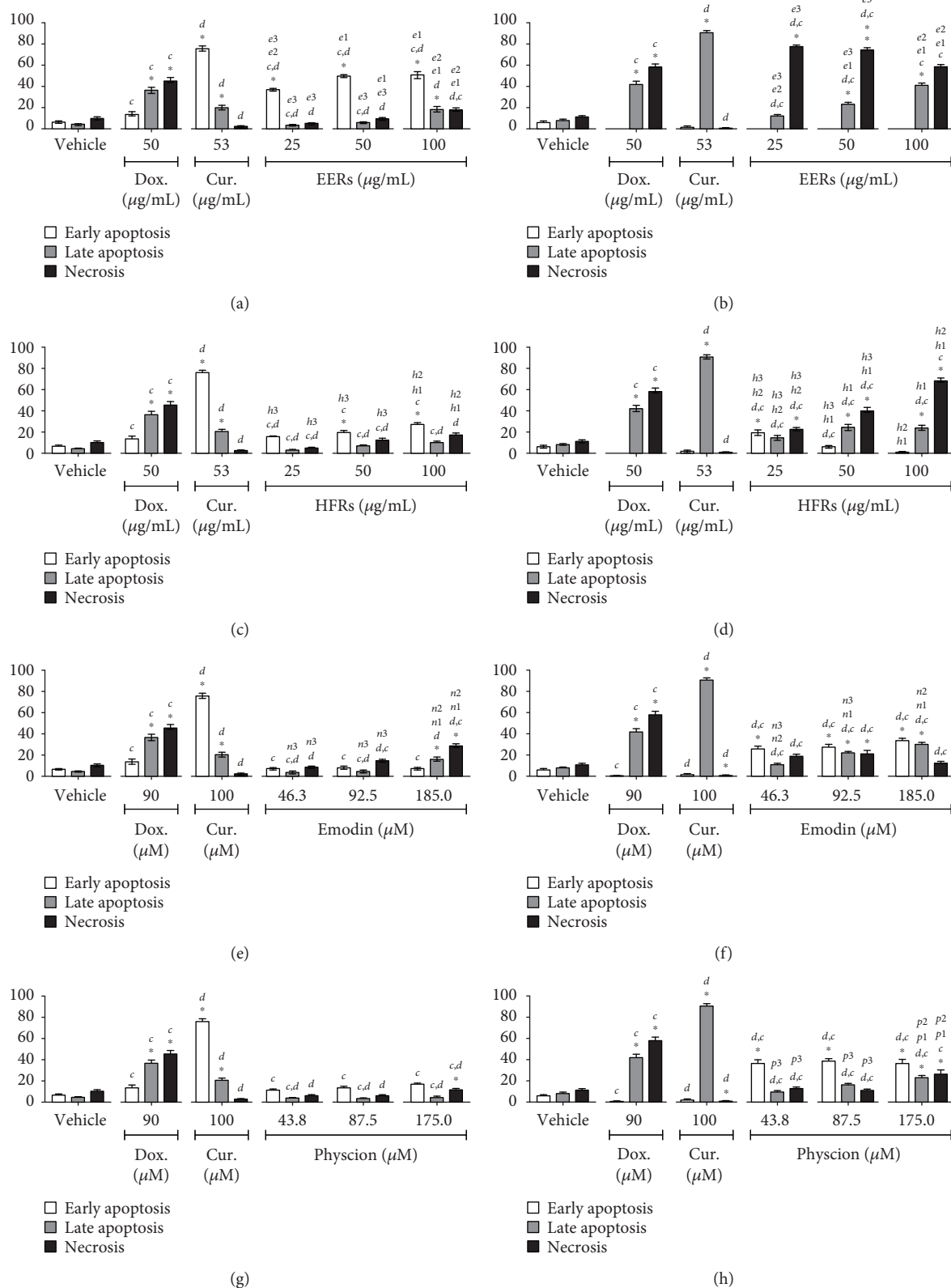


FIGURE 3: Cell death analysis in HSC-3 cells. Cytomorphological viability assay for (a) EERs, (c) HFRs, (e) emodin, and (g) physcion. Annexin-V assay for (b) EERs, (d) HFRs, (f) emodin, and (h) physcion. Comparison with significant statistical differences between treatments: vehicle (*); doxorubicin (d); curcumin (c); EERs: 25 µg/mL (e1); EERs: 50 µg/mL (e2); EERs: 100 µg/mL (e3); HFRs: 25 µg/mL (h1); HFRs: 50 µg/mL (h2); HFRs: 100 µg/mL (h3); emodin: 46.3 µM (n1); emodin: 92.8 µM (n2); emodin: 185.0 µM (n3); physcion: 43.8 µM (p1); physcion: 87.5 µM (p2); physcion: 175.0 µM (p3); and cell status: early apoptosis, late apoptosis, and necrosis. Results are expressed as mean of three independent experiments \pm standard error ($M \pm SE$), analyzed by one-way ANOVA with Tukey's posttest, $p \leq 0.05$.

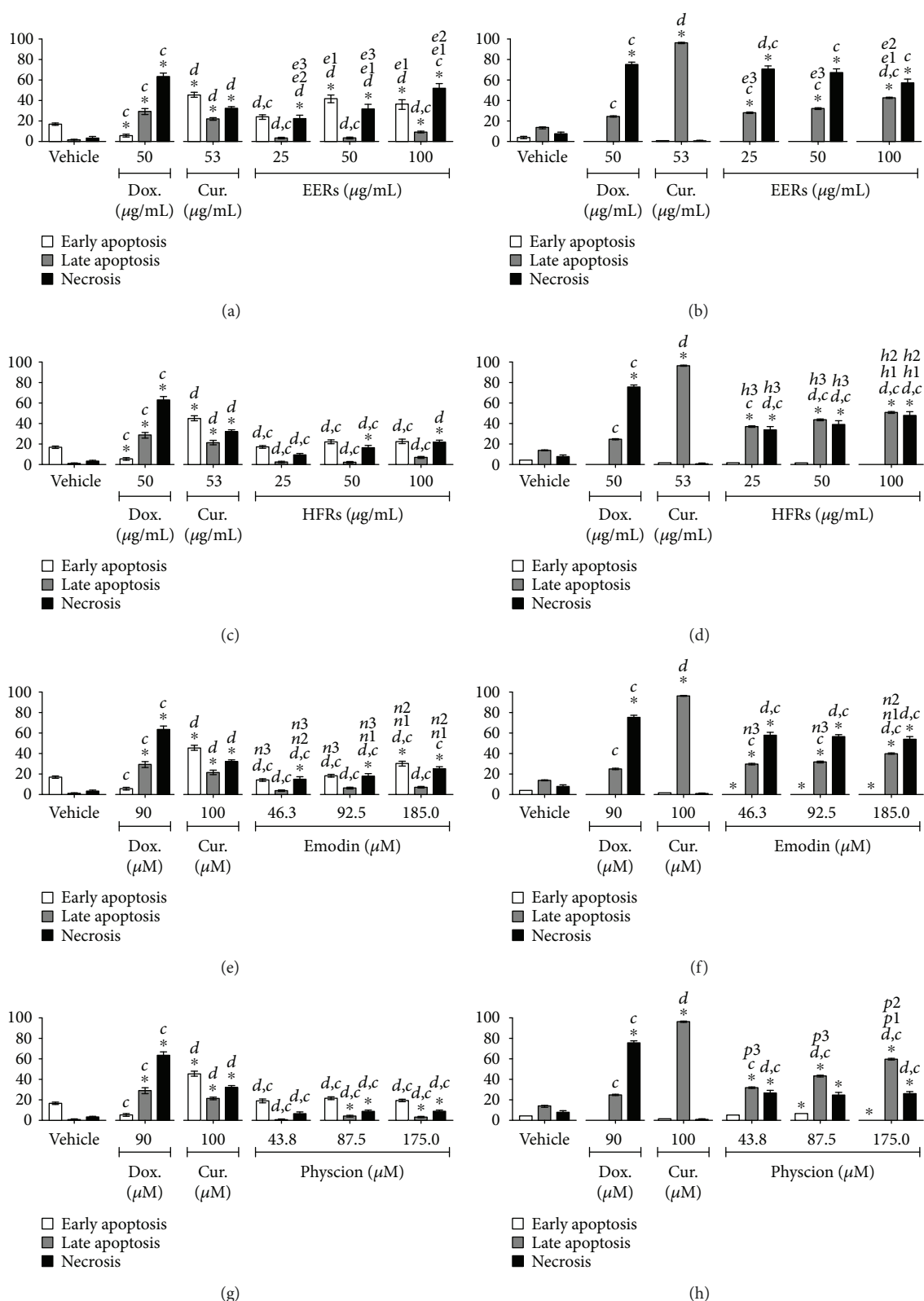


FIGURE 4: Cell death analysis in HaCaT cells. Cyto-morphological viability assay for (a) EERs, (c) HFRs, (e) emodin, and (g) physcion. Annexin-V assay for (b) EERs, (d) HFRs, (f) emodin, and (h) physcion. Comparison with significant statistical differences between treatments: vehicle (*); doxorubicin (d); curcumin (c); EERs: 25 $\mu\text{g/mL}$ (e1); EERs: 50 $\mu\text{g/mL}$ (e2); EERs: 100 $\mu\text{g/mL}$ (e3); HFRs: 25 $\mu\text{g/mL}$ (h1); HFRs: 50 $\mu\text{g/mL}$ (h2); HFRs: 100 $\mu\text{g/mL}$ (h3); emodin: 46.3 μM (n1); emodin: 92.8 μM (n2); emodin: 185.0 μM (n3); physcion: 43.8 μM (p1); physcion: 87.5 μM (p2); physcion: 175.0 μM (p3); and cell status: early apoptosis, late apoptosis, and necrosis. Results are expressed as mean of three independent experiments \pm standard error ($M \pm SE$), analyzed by one-way ANOVA with Tukey's post-test, $p \leq 0.05$.

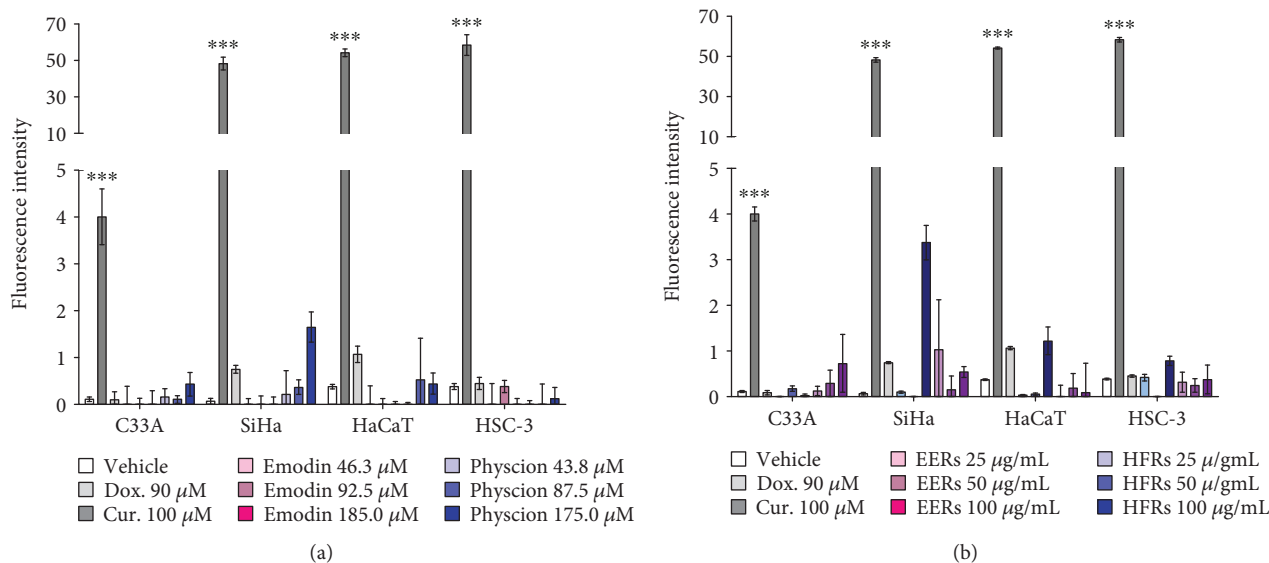


FIGURE 5: Caspase 3 activity assay. SiHa, C33A, HSC-3, and HaCaT after treatment for 6 h with (a) emodin, physcion and (b) EERs and HFRs. Results are expressed as mean cell fluorescence intensity of three independent experiments ± standard error ($M \pm SE$), analyzed by one-way ANOVA with Tukey's post-test (statistically significant difference compared to vehicle control group: *** $p \leq 0.001$).

of treatment, and in an oral cell line (HSC-3) and immortalized keratinocytes (HaCaT) after 12 h of treatment.

3.4. Emodin, Physcion, and EERs Increased Intracellular Oxidative Stress. Under normal physiological conditions, cells maintain a balance between oxidant species and antioxidants, referred to as redox homeostasis. At low concentrations, RONS act to regulate proliferation, cell death, and other metabolic processes [59]. An increase in oxidative stress has been associated with several types of cell death, including oxeiptosis, a recently described cell death pathway exhibiting the morphological features of apoptosis that is independent of caspase activation [60].

Studies have associated the toxic effect of emodin and physcion with an increase in intracellular RONS, which thereby promotes deregulation of mitochondrial membrane potential and activation of cell death [50, 52, 53, 56]. Therefore, the levels of thiobarbituric acid reactive species (TBARS) were quantified after the treatment of the cells with emodin, physcion, and EERs.

Emodin promoted an increase in TBARS levels when compared with the control (DMSO 0.5%, v/v) in all cell lines, but in C33A and HSC-3, only the highest emodin concentration promoted a significant increase. Only the highest concentration of physcion caused a significant increase in TBARS levels in SiHa, C33A, and HaCaT, and no changes were observed in HSC-3. In SiHa, C33A, and HaCaT, EERs promoted an increase in TBARS, whereas in HSC-3, a lower concentration of EERs promoted a decrease in TBARS (Figure 6).

The redox status of transformed cells is significantly influenced by the levels of RONS such as $O_2^{\bullet-}$, H_2O_2 , $\bullet NO$, and $HOCl/OCl^-$, and by the expression of enzymes such as NOX-1, SOD, and catalase in the cell membrane, promoting proliferation stimuli and inhibiting the deleterious effects of these reactive species. It is known that $\bullet NO$ can induce cell

death at some levels, as can the product of its reaction with $O_2^{\bullet-}$, $ONOO^-$. In addition, $\bullet NO$ is able to inactivate catalase, leading to changes in the H_2O_2 levels; catalase can be reactivated by $O_2^{\bullet-}$, releasing $\bullet NO$ and the active enzyme, thus inducing cell death via $HOCl/OCl^-$ and $\bullet NO/ONOO^-$ [44, 45, 61]. We found that upon treating the cells with emodin and physcion, these compounds can interact with extra- and intracellular RONS (mainly $O_2^{\bullet-}$ and $\bullet NO$), altering H_2O_2 and $\bullet NO$ concentrations, thus unbalancing the performance of these enzymes. In addition to the effect on cell redox homeostasis, the formation of the respective semi-quinones can also cause lipoperoxidation, corroborated by an increase in TBARS and heightened DNA damage.

Su et al. [50] observed a decrease in the cytotoxic effects of emodin after the pretreatment of A549 cells with the antioxidants ascorbic acid and N-acetyl cysteine. In addition, an increase in the concentrations of RONS promoted by the glycosylated form of physcion in HepG2 cells induced the activation of AMP-activated protein kinase (AMPK), resulting in the downregulation of DNA methyltransferase 1 (DNMT1), which is mediated by the transcription factor Sp1. DNMT1 is responsible for DNA methylation; its elevated expression has been reported to cause silencing of some tumor suppressor genes in various types of carcinomas [56].

3.5. Emodin, Physcion, and Chrysophanol Promoted Irreparable Damage to the DNA of Cervical Cancer Cells. The anthraquinones chrysophanol, emodin, and physcion were mutagenic only in SiHa and C33A cells after 24 h of treatment at all tested concentrations, except for chrysophanol, which was mutagenic only at a lower concentration. In HSC-3 and HaCaT cells, only the treatment with hydrogen peroxide (positive control) showed an increase in chromosomal aberrations. These results are shown in Table 3. HaCaT is a nontumoral immortalized cell line with p53 mutations

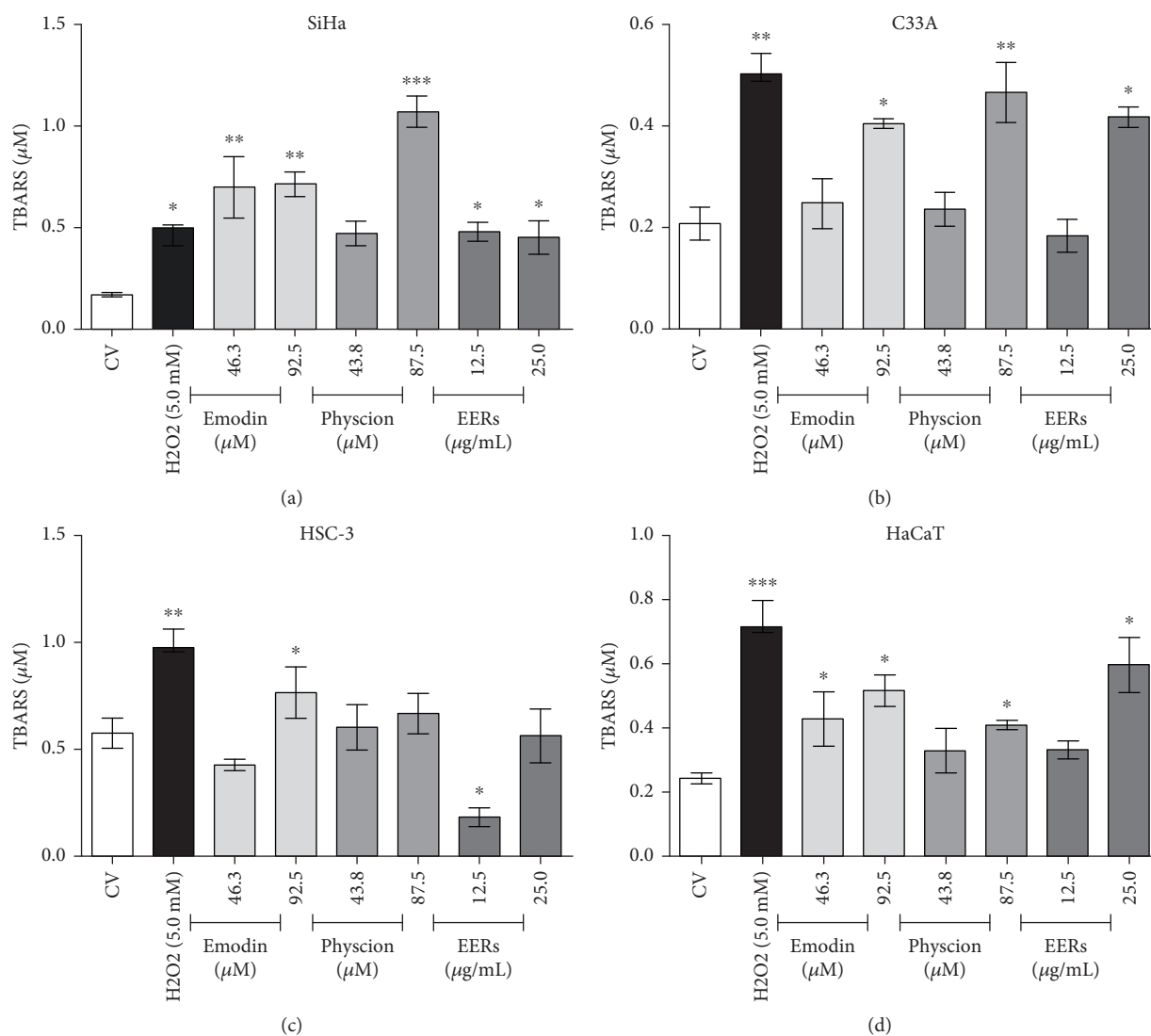


FIGURE 6: TBARS assay in SiHa, C33A, HSC-3, and HaCaT. 24-hour treatment with emodin, physcion, and EERs. H₂O₂ as positive control (5.0 mM). Results are expressed as mean of TBARS concentration (product formed after the reaction of the extracellular medium with thiobarbituric acid in at 95°C for 60 min) of three independent experiments \pm standard error ($M \pm SE$), analyzed by one-way ANOVA and Newman-Keuls post-test (statistically significant difference compared to the vehicle control group: * $p \leq 0.05$; ** $p \leq 0.01$; *** $p \leq 0.001$).

that generate an unlimited proliferation phenotype [62]. On the other hand, HSC-3, SiHa, and C33A are tumoral lines, with high rates of genomic instability, intense proliferative characteristics, and high invasiveness capacities [5, 7, 8].

The comet assay (Figure 7) was carried out in SiHa and C33A to verify the induction of reversible damage (DNA strand breaks). Only emodin showed significant genotoxicity in SiHa, but not in C33A cells. Taken together, data from the micronuclei and comet assays suggested that chrysophanol and physcion caused irreversible mutagenic damage by promoting errors during cell division (e.g., increase in micronuclei formation). On the other hand, emodin caused reversible breaks in DNA strands in the SiHa cell line, while also promoting chromosomal segregation errors (e.g., increase in micronuclei formation). Therefore, the damage promoted by emodin in SiHa cell DNA is more intense than that induced by chrysophanol and physcion. Furthermore, under

conditions of oxidative stress, certain biomolecules are relevant targets of RONS, including DNA. The enzyme poly (ADP-ribose) polymerase 1 (PARP-1) binds to damaged DNA to catalyze protein ADP-ribosylation using NAD⁺ to initiate DNA repair. When the damage is limited, the DNA can be repaired and NAD⁺ levels are regenerated using ATP; however, if the DNA damage is not repaired, the cells die by apoptosis in a caspase-dependent manner. On the other hand, when damage is extensive, the sustained activation of PARP-1 depletes NAD⁺ and ATP stores; the cells are unable to activate the caspase pathway, which are ATP-dependent, and necrosis occurs [63]. Thus, the excessive activation of PARP-1 to repair the extensive DNA damage (verified in the micronuclei and comet assay), induced by the oxidative stress provoked by the treatment with emodin and physcion, may be related to caspase-independent cell death. Also, activation of PARP-1 increases

TABLE 3: Micronuclei assay.

	SiHa	Micronuclei frequency (%)		
		C33A	HSC-3	HaCaT
DMSO (1%, v/v)	0.939 ± 0.09	0.617 ± 0.03	4.16 ± 0.54	0.177 ± 0.02
H ₂ O ₂ (0.1 mM)	1.916 ± 0.32*	1.190 ± 0.16**	9.33 ± 0.63*	1.198 ± 0.27***
<i>Chrysophanol</i>				
3.125 µg/mL (12.3 µM)	3.894 ± 0.33***	0.757 ± 0.20	3.913 ± 0.69	0.228 ± 0.18
6.25 µg/mL (24.5 µM)	2.832 ± 0.21***	1.129 ± 0.05**	2.655 ± 0.063	0.066 ± 0.02
12.5 µg/mL (49.1 µM)	2.431 ± 0.2**	1.403 ± 0.07***	2.706 ± 0.9	0.151 ± 0.09
<i>Emodin</i>				
3.125 µg/mL (11.6 µM)	2.120 ± 0.13*	0.932 ± 0.08*	4.720 ± 0.82	0.181 ± 0.06
6.25 µg/mL (23.2 µM)	2.428 ± 0.36**	1.318 ± 0.13***	4.246 ± 1.23	0.296 ± 0.16
12.5 µg/mL (46.3 µM)	3.528 ± 0.19***	1.081 ± 0.04**	2.789 ± 1.63	0.102 ± 0.018
<i>Physcion</i>				
3.125 µg/mL (10.9 µM)	1.699 ± 0.26*	1.298 ± 0.06**	5.723 ± 0.96	0.478 ± 0.21
6.25 µg/mL (21.9 µM)	1.990 ± 0.27*	1.246 ± 0.12**	4.794 ± 1.02	0.421 ± 0.091
12.5 µg/mL (43.8 µM)	1.896 ± 0.17*	1.143 ± 0.15**	4.915 ± 0.76	0.239 ± 0.19

Hydrogen peroxide (0.1 mM) as positive control and DMSO (1%, v/v) as vehicle control. Mean ± standard error of the number of micronuclei found in three independent experiments on cells. All cells were analyzed by the IN Cell Analyzer 2000 (GE Healthcare) software. (* $p \leq 0.05$; ** $p \leq 0.01$; *** $p \leq 0.001$ compared to vehicle control analyzed by ANOVA and Newman-Keuls post-test).

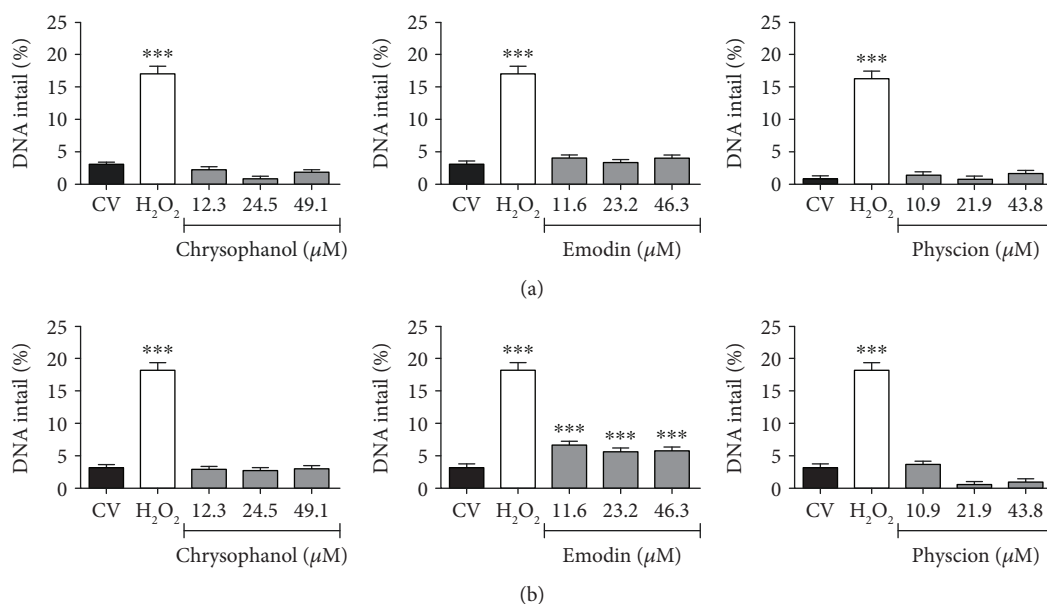


FIGURE 7: Comet assay for (a) C33A and (b) SiHa. Evaluation of genotoxicity of chrysophanol, emodin, and physcion. H₂O₂ (0.1 mM) as positive control and CV: vehicle control (1% DMSO). (***) = statistically significant difference for $p \leq 0.001$, analyzed by Kruskal-Wallis and Dunn's post-test).

the AMP/ATP ratio, activating the AMP-activated protein kinase (AMPK), which in turns inhibits mTORC1, leading to inhibition of anabolic processes and stimulation of catabolic events, which could also be contributing to cell death responses [64].

3.6. Emodin, Physcion, and EERs Changed the Levels of BAX and BCL-2 in SiHa Cells and the Levels of Caspase-3 in SiHa, C33A, HSC-3, and HaCaT Cells. The levels of BAX

and BCL-2 were studied only in the SiHa cell line, and the levels of caspase-3 were evaluated in all studied cells. In SiHa, the levels of BCL-2 (antiapoptotic protein) were decreased after treatment with emodin across all tested concentrations and after treatment with EERs at only the highest concentration, corroborating the cell death experiments where apoptosis and necrosis were observed. The levels of BAX (proapoptotic protein) were increased after treatment with 92.5 µM emodin, whereas treatment with EERs caused a

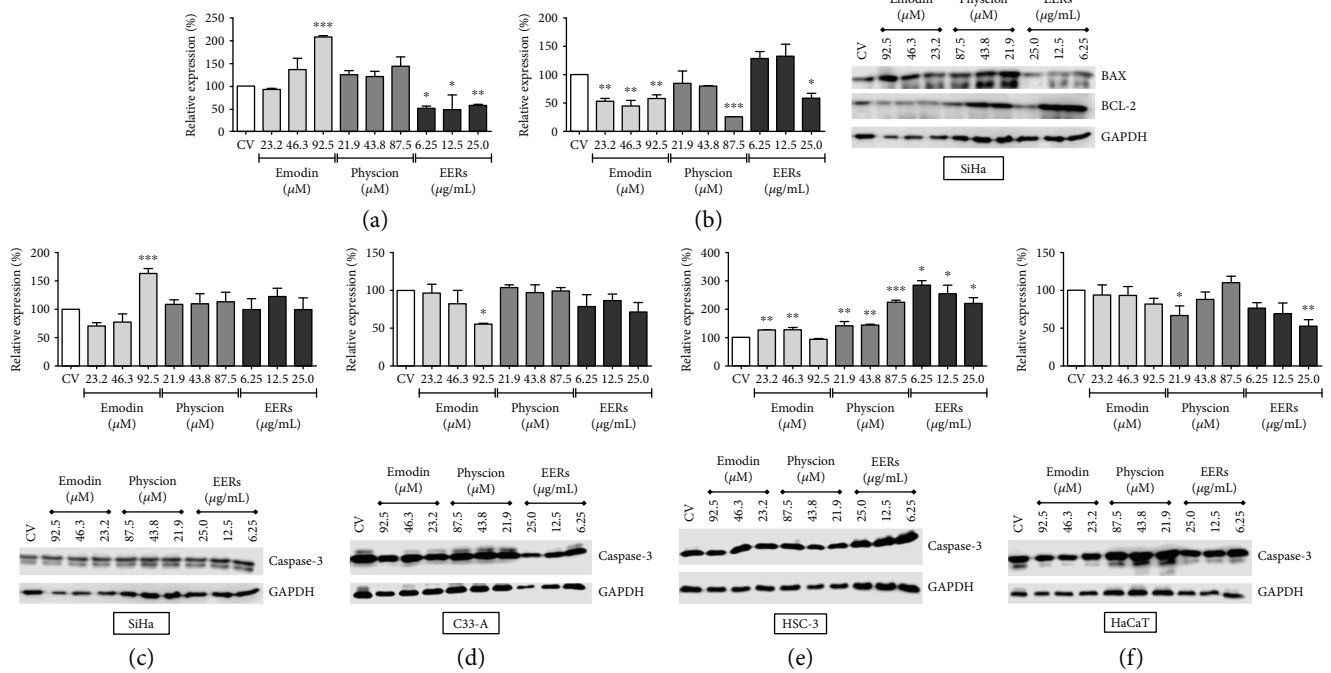


FIGURE 8: Levels of BAX, BCL-2, and caspases-3. (a) BAX, (b) BCL-2, (c) caspases-3 for SiHa, (d) caspases-3 for C33A, (e) caspases-3 for HSC-3, and (f) caspases-3 for HaCaT. Results are expressed as mean of electrophoretic bands densitometry, corrected for the control of cells treated with DMSO 0.5% (v/v) (CV), of two independent experiments \pm standard error ($M \pm SE$), analyzed by one-way ANOVA with Newman-Keuls post-test (statistically significant difference compared to CV: * $p \leq 0.05$; ** $p \leq 0.01$; *** $p \leq 0.001$).

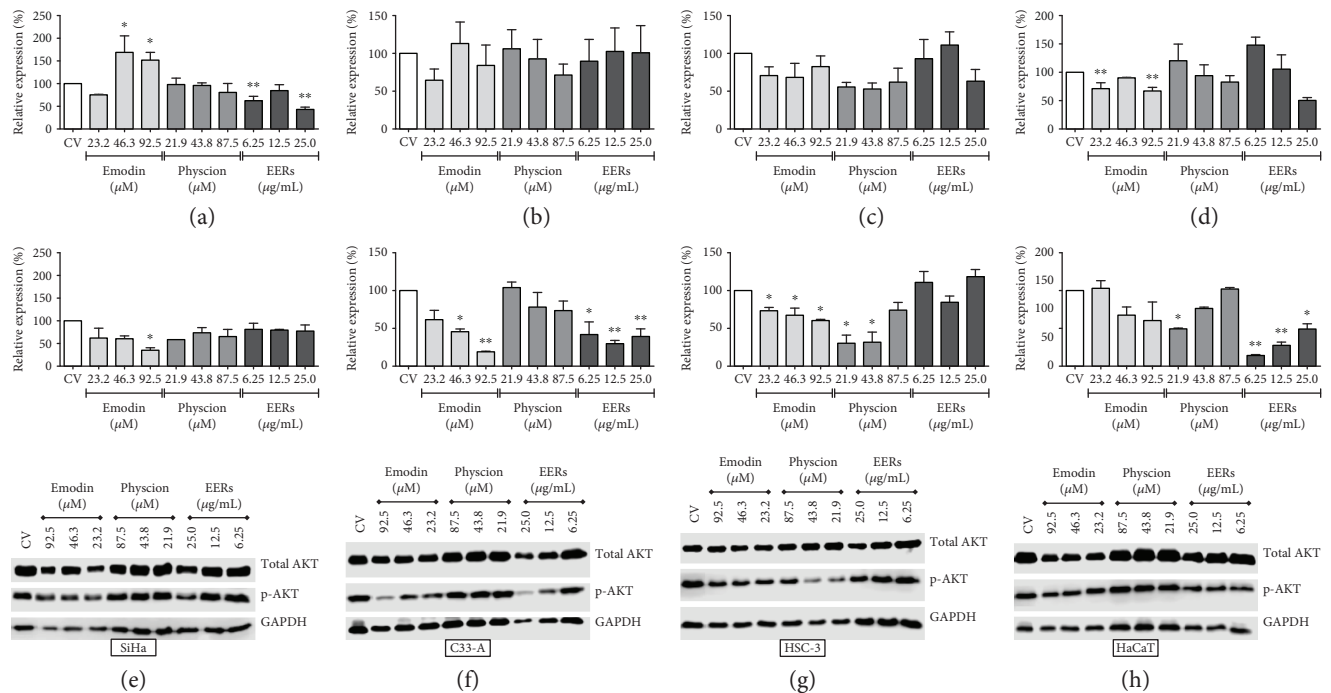


FIGURE 9: Total protein and phosphorylation (Ser-473 residue) levels of AKT. (a) Total AKT and (b) p-Ser-473-AKT for SiHa; (c) total AKT and (d) p-Ser-473-AKT for C33A; (e) total AKT and (f) p-Ser-473-AKT for HSC-3 (g); total AKT and (h) p-Ser-473-AKT for HaCaT. Results are expressed as mean of electrophoretic bands densitometry, corrected for the control of cells treated with DMSO 0.5% (v/v) (CV), of two independent experiments \pm standard error ($M \pm SE$), analyzed by one-way ANOVA with Newman-Keuls post-test (statistically significant difference compared to CV: * $p \leq 0.05$; ** $p \leq 0.01$).

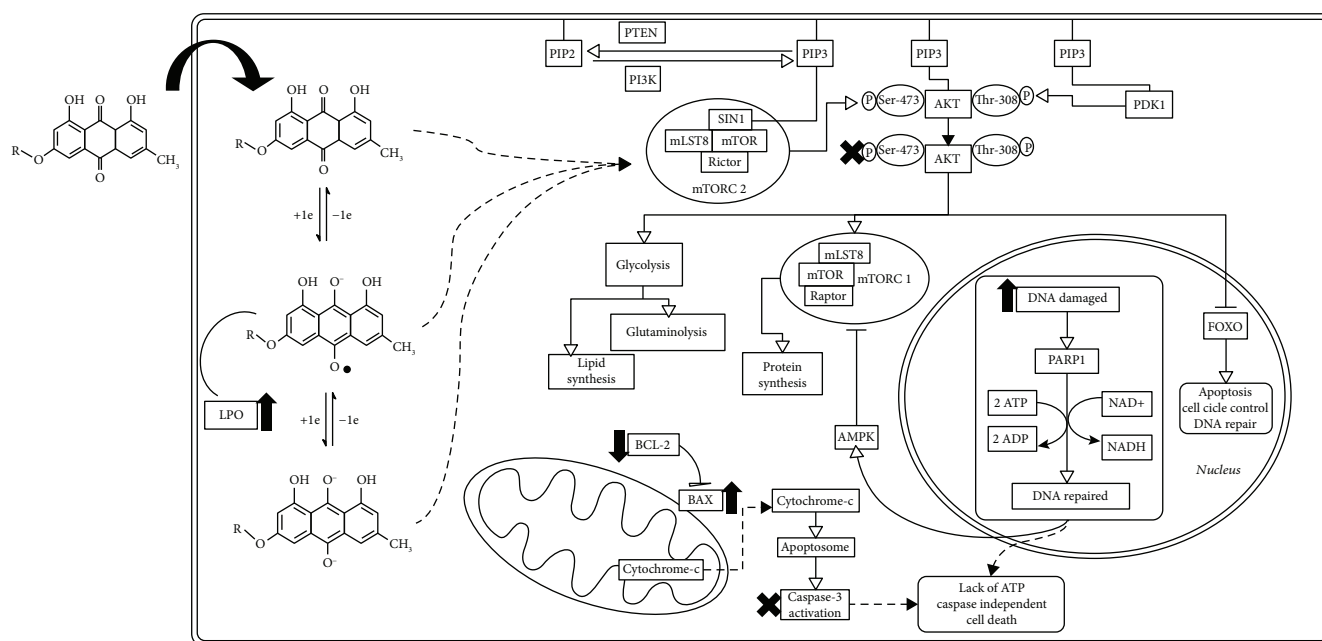


FIGURE 10: Hypothesis of the mechanisms causing cancer cell death induced by emodin and physcion. The intracellular oxidative environment stimulates the conversion of the anthraquinones (emodin, R=H, and physcion, R=OCH₃) into their semiquinone forms, which may be causing both lipoperoxidation (LPO) and DNA damage and this last activating repair enzymes (e.g., PARP-1) and consequently increasing the ATP consumption. Anthraquinones could also be promoting an inhibition of metabolic processes important to cell survival and proliferation, via inhibition of AKT; this causes activation of FOXO factors, stimulation of cell cycle control, DNA repair, and activation of cell death pathways. The increased ATP consumption could also lead to AMPK activation, which inhibits anabolic pathways and activates catabolic processes. Taken together, the oxidative stress generated by the anthraquinones and the inhibition of AKT could both lead to loss of the metabolic profile favoring tumor survival and an imbalance in BAX and BCL-2 levels, resulting in induction of cell death via apoptosis and necrosis, independent of caspase-3 activation.

decrease in BAX levels (Figure 8). Furthermore, the decrease in BAX levels observed upon treatment with EERs may be related to autophagy-induced cell death, since the decrease in apoptotic modulators such as BAX has been associated with autophagic cell death. Known as type II cell death, it occurs via activation of cathepsins, without caspase activation [49]. Caspase-3 levels increased in the HSC-3 cells treated with emodin, physcion, and EERs. In SiHa, only emodin at its highest concentration increased the levels of caspase-3. Interestingly, emodin decreased the levels of caspase-3 in both C33A and HaCaT cells (Figure 8).

3.7. Emodin, Physcion, and EERs Inhibited AKT. Emodin reduced the AKT phosphorylation levels of the serine-473 residue with at least one of the three tested concentrations in all tumor cell lines, most effectively in HSC-3, followed by C33A and SiHa, without promoting significant changes in the normal cell line (HaCaT) (Figure 9). Corroborating our findings, studies demonstrated that emodin promoted a decrease in the phosphorylation of AKT in A549 [50], SMMC-7721 [51], and HepG2 cells [52].

Physcion did not promote significant changes in AKT phosphorylation levels in cervical tumor cells (SiHa and C33A) but significantly reduced AKT phosphorylation in HSC-3 cells at the two lowest concentrations and in HaCaT cells at the lowest concentration (Figure 9). EERs reduced AKT phosphorylation in C33A and HaCaT cells at all tested concentrations; however, it did not promote significant

changes in AKT phosphorylation in HSC-3 and SiHa cells (Figure 9).

The PI3K/AKT pathway is closely associated with proliferative signals triggered by mTOR (mammalian target of rapamycin). mTOR acts via two protein complexes: mTORC1, which is activated by AKT, and mTORC2, which in turn activates AKT via phosphorylation at the Ser-473 residue [65]. HSC-3 cells have mutations in PIK3CA that cause increases in AKT phosphorylation, while SiHa cells exhibit high expression levels of PIK3CA and, consequently, increased PI3K activity. The C33A cell line has a mutation in the catalytic subunit of PI3K which results in increased PI3K activity and, consequently, strong AKT activation. C33A cells also have a mutation in the gene, silencing its expression and thereby culminating in a further increase in the PI3K and AKT activity [7]. Interestingly, emodin and EERs were able to reduce AKT activation in C33A cells, that is, in a cell line that is characterized by superstimulation of this pathway. Moreover, the imbalance in the PI3K/AKT pathway is associated with cell death in different tumor cells, thereby emerging as a potential target for cancer treatment [66–69].

4. Conclusion

In summary, the anthraquinones emodin and physcion and the crude extracts and fractions of *Rhamnus sphaerosperma* var. *pubescens* induced cell death in both cervical and oral

squamous cancer cells, likely by inducing multiple cellular events including increased oxidative stress, DNA damage, and inhibition of AKT (Figure 10). Taken together, the present findings highlight the promising anticancer activity of anthraquinones from *Rhamnus sphaerosperma*, supporting the need for ongoing investigations, mainly with emodin and physcion, contributing to the search of new therapeutic opportunities for cervical and oral squamous carcinomas.

Abbreviations

EERs:	Ethanol crude extract from stems of <i>Rhamnus sphaerosperma</i> var. <i>pubescens</i>
HFRs:	Hexanic fraction
CFRs:	Chloroform fraction
EAFRs:	Ethyl acetate fraction
PI3K:	Phosphatidylinositol-3-kinase
AKT:	Protein kinase B
PTEN:	Phosphatase and tensin homolog
PDK-1:	Pyruvate dehydrogenase kinase 1
mTORC2:	Mammalian target of rapamycin complex 2
RONS:	Reactive oxygen and nitrogen species
SOD:	Superoxide dismutase
NOX-1:	NADPH oxidase 1
DUOX-POD:	Dual oxidase with peroxidase domain
$O_2^{\bullet-}$:	Superoxide anion
H_2O_2 :	Hydrogen peroxide
$\bullet NO$:	Nitric oxide
HOCl/OCl ⁻ :	Hypochlorous acid/hypochlorite anion
TBARS:	Thiobarbituric acid reactive species.

Data Availability

The authors confirm that the data supporting the findings of this study are available within the article.

Conflicts of Interest

The authors declare that there are no conflicts of interest.

Acknowledgments

The authors would like to thank the Sao Paulo Research Foundation (FAPESP), the National Council for Scientific and Technological Development (CNPq), and the Scientific Support and Development Program of the School of Pharmaceutical Sciences of UNESP (PADC/FCFAR, UNESP) for financial support.

References

- [1] L. A. Torre, F. Bray, R. L. Siegel, J. Ferlay, J. Lortet-Tieulent, and A. Jemal, "Global cancer statistics, 2012," *CA: A Cancer Journal for Clinicians*, vol. 65, no. 2, pp. 87–108, 2015.
- [2] Z. Surviladze, R. T. Sterk, S. A. DeHaro, and M. A. Ozbun, "Cellular entry of human papillomavirus type 16 involves activation of the phosphatidylinositol 3-kinase/Akt/mTOR pathway and inhibition of autophagy," *Journal of Virology*, vol. 87, no. 5, pp. 2508–2517, 2013.
- [3] J. Ferlay, I. Soerjomataram, R. Dikshit et al., "Cancer incidence and mortality worldwide: sources, methods and major patterns in GLOBOCAN 2012," *International Journal of Cancer*, vol. 136, no. 5, pp. E359–E386, 2015.
- [4] L. Zhang, J. Wu, M. T. Ling, L. Zhao, and K. N. Zhao, "The role of the PI3K/Akt/mTOR signalling pathway in human cancers induced by infection with human papillomaviruses," *Molecular Cancer*, vol. 14, no. 1, pp. 87–13, 2015.
- [5] K. Kozaki, I. Imoto, A. Pimkhaokham et al., "PIK3CA mutation is an oncogenic aberration at advanced stages of oral squamous cell carcinoma," *Cancer Science*, vol. 97, no. 12, pp. 1351–1358, 2006.
- [6] Y.-Y. Ma, S.-J. Wei, Y.-C. Lin et al., "PIK3CA as an oncogene in cervical cancer," *Oncogene*, vol. 19, no. 23, pp. 2739–2744, 2000.
- [7] R. Rashmi, C. DeSelm, C. Helms et al., "AKT inhibitors promote cell death in cervical cancer through disruption of mTOR signaling and glucose uptake," *PLoS One*, vol. 9, no. 4, article e92948, 2014.
- [8] J. Jin, Z. Zhang, S. Zhang et al., "Fatty acid binding protein 4 promotes epithelial-mesenchymal transition in cervical squamous cell carcinoma through AKT/GSK3 β /snail signaling pathway," *Molecular and Cellular Endocrinology*, vol. 461, pp. 155–164, 2018.
- [9] R. G. Jones and C. B. Thompson, "Tumor suppressors and cell metabolism: a recipe for cancer growth," *Genes & Development*, vol. 23, no. 5, pp. 537–548, 2009.
- [10] P. Liu, H. Cheng, T. M. Roberts, and J. J. Zhao, "Targeting the phosphoinositide 3-kinase pathway in cancer," *Nature Reviews. Drug Discovery*, vol. 8, no. 8, pp. 627–644, 2009.
- [11] M. Kollareddy, E. Dimitrova, K. C. Vallabhaneni et al., "Regulation of nucleotide metabolism by mutant p53 contributes to its gain-of-function activities," *Nature Communications*, vol. 6, no. 1, pp. 7389–7313, 2015.
- [12] C. A. Sparks and D. A. Guertin, "Targeting mTOR: prospects for mTOR complex 2 inhibitors in cancer therapy," *Oncogene*, vol. 29, no. 26, pp. 3733–3744, 2010.
- [13] R. A. Cairns, I. S. Harris, and T. W. Mak, "Regulation of cancer cell metabolism," *Nature Reviews. Cancer*, vol. 11, no. 2, pp. 85–95, 2011.
- [14] X. Zhang, N. Tang, T. J. Hadden, and A. K. Rishi, "Akt, FoxO and regulation of apoptosis," *Biochimica et Biophysica Acta (BBA) - Molecular Cell Research*, vol. 1813, no. 11, pp. 1978–1986, 2011.
- [15] A. Gupta, S. Anjomani-Virmouni, N. Koundouros et al., "PARK2 depletion connects energy and oxidative stress to PI3K/Akt activation via PTEN S-nitrosylation," *Molecular Cell*, vol. 65, no. 6, pp. 999–1013.e7, 2017.
- [16] J. D. Lambeth, T. Kawahara, and B. Diebold, "Regulation of Nox and Duox enzymatic activity and expression," *Free Radical Biology & Medicine*, vol. 43, no. 3, pp. 319–331, 2007.
- [17] L. Alberghina and D. Gaglio, "Redox control of glutamine utilization in cancer," *Cell Death & Disease*, vol. 5, no. 12, pp. e1561–e1569, 2014.
- [18] G. Chen, J. Wu, N. Li, and M. Guo, "Screening for anti-proliferative and anti-inflammatory components from *Rhamnus davurica* Pall. Using bio-affinity ultrafiltration with multiple drug targets," *Analytical and Bioanalytical Chemistry*, vol. 410, no. 15, pp. 3587–3595, 2018.
- [19] R. B. Ammar, A. Neffati, I. Skandrani et al., "Anti-lipid peroxidation and induction of apoptosis in the erythroleukaemic cell

- line K562 by extracts from (Tunisian) *Rhamnus alaternus* L. (Rhamnaceae),” *Natural Product Research*, vol. 25, no. 11, pp. 1047–1058, 2011.
- [20] R. B. Ammar, M. B. Sghaier, J. Boubaker et al., “Antioxidant activity and inhibition of aflatoxin B₁-, nifuroxazide-, and sodium azide-induced mutagenicity by extracts from *Rhamnus alaternus* L,” *Chemico-Biological Interactions*, vol. 174, no. 1, pp. 1–10, 2008.
 - [21] T. F. Moreira, D. M. Deoliveira, M. F. Arruda et al., “Lipid peroxidation inhibition by ethanolic extract and fractions from *Rhamnus sphaerosperma* var. *pubescens* (Reissek) M.C. Johnst. (Rhamnaceae),” *International Journal of Phytomedicine*, vol. 5, no. 2, pp. 136–140, 2013.
 - [22] I. Manet, F. Manoli, B. Zambelli et al., “Complexes of the antitumoral drugs doxorubicin and sabarubicin with telomeric G-quadruplex in basket conformation: ground and excited state properties,” *Photochemical & Photobiological Sciences*, vol. 10, no. 8, pp. 1326–1337, 2011.
 - [23] B. Hazra, S. Biswas, and N. Mandal, “Antioxidant and free radical scavenging activity of *Spondias pinnata*,” *BMC Complementary and Alternative Medicine*, vol. 8, no. 1, p. 63, 2008.
 - [24] J. C. Morris, “The acid ionization constant of HOCl from 5 to 35°,” *The Journal of Physical Chemistry*, vol. 70, no. 12, pp. 3798–3805, 1966.
 - [25] J. Dypbukt, C. Bishop, W. Brooks, B. Thong, H. Eriksson, and A. Kettle, “A sensitive and selective assay for chloramine production by myeloperoxidase,” *Free Radical Biology & Medicine*, vol. 39, no. 11, pp. 1468–1477, 2005.
 - [26] A. J. Kettle and C. C. Winterbourn, “[53] Assays for the chlorination activity of myeloperoxidase,” *Methods in Enzymology*, vol. 233, pp. 502–512, 1994.
 - [27] J. M. Zgliczyński, T. Stelmazyńska, J. Domański, and W. Ostrowski, “Chloramines as intermediates of oxidation reaction of amino acids by myeloperoxidase,” *Biochimica et Biophysica Acta (BBA)—Enzymology*, vol. 235, no. 3, pp. 419–424, 1971.
 - [28] G.-C. Yen, H.-H. Lai, and H.-Y. Chou, “Nitric oxide-scavenging and antioxidant effects of *Uraria crinita* root,” *Food Chemistry*, vol. 74, no. 4, pp. 471–478, 2001.
 - [29] Y. Hashimoto, Y. Shimada, A. Itami et al., “Growth inhibition through activation of peroxisome proliferator-activated receptor γ in human oesophageal squamous cell carcinoma,” *European Journal of Cancer*, vol. 39, no. 15, pp. 2239–2246, 2003.
 - [30] R. A. Duarte, E. R. Mello, C. Araki et al., “Alkaloids extracted from *Pterogyne nitens* induce apoptosis in malignant breast cell line,” *Tumor Biology*, vol. 31, no. 5, pp. 513–522, 2010.
 - [31] W. C. Earnshaw, L. M. Martins, and S. H. Kaufmann, “Mammalian caspases: structure, activation, substrates, and functions during apoptosis,” *Annual Review of Biochemistry*, vol. 68, no. 1, pp. 383–424, 1999.
 - [32] O. H. Lowry, N. Rosebrough, A. Farr, and R. Randall, “Protein measurement with the folin phenol reagent,” *The Journal of Biological Chemistry*, vol. 193, no. 1, pp. 265–275, 1951.
 - [33] U. K. Laemmli, “Cleavage of structural proteins during the assembly of the head of bacteriophage T4,” *Nature*, vol. 227, no. 5259, pp. 680–685, 1970.
 - [34] H. Towbin, T. Staehelin, and J. Gordon, “Electrophoretic transfer of proteins from polyacrylamide gels to nitrocellulose sheets: procedure and some applications,” *Proceedings of the National Academy of Sciences of the United States of America*, vol. 76, no. 9, pp. 4350–4354, 1979.
 - [35] C. Haan and I. Behrmann, “A cost effective non-commercial ECL-solution for Western blot detections yielding strong signals and low background,” *Journal of Immunological Methods*, vol. 318, no. 1–2, pp. 11–19, 2007.
 - [36] N. D. Md Zamri, M. U. Imam, S. A. Abd Ghafar, and M. Ismail, “Antioxidative effects of germinated brown rice-derived extracts on H₂O₂-induced oxidative stress in HepG2 cells,” *Evidence-based Complementary and Alternative Medicine*, vol. 2014, Article ID 371907, 11 pages, 2014.
 - [37] A. Shibai-Ogata, C. Kakinuma, T. Hioki, and T. Kasahara, “Evaluation of high-throughput screening for *in vitro* micronucleus test using fluorescence-based cell imaging,” *Mutagenesis*, vol. 26, no. 6, pp. 709–719, 2011.
 - [38] N. P. Singh, M. T. McCoy, R. R. Tice, and E. L. Schneider, “A simple technique for quantitation of low levels of DNA damage in individual cells,” *Experimental Cell Research*, vol. 175, no. 1, pp. 184–191, 1988.
 - [39] R. R. Tice, E. Agurell, D. Anderson et al., “Single cell gel/comet assay: guidelines for *in vitro* and *in vivo* genetic toxicology testing,” *Environmental and Molecular Mutagenesis*, vol. 35, no. 3, pp. 206–221, 2000.
 - [40] P. Moller, “The alkaline comet assay: towards validation in biomonitoring of DNA damaging exposures,” *Basic & Clinical Pharmacology & Toxicology*, vol. 98, no. 4, pp. 336–345, 2006.
 - [41] R. S. Gonçalves, E. L. Silva, N. Hioka, C. V. Nakamura, M. L. Bruschi, and W. Caetano, “An optimized protocol for anthraquinones isolation from *Rhamnus frangula* L,” *Natural Product Research*, vol. 32, no. 3, pp. 366–369, 2017.
 - [42] A. B. Kunnumakkara, D. Bordoloi, C. Harsha, K. Banik, S. C. Gupta, and B. B. Aggarwal, “Curcumin mediates anticancer effects by modulating multiple cell signaling pathways,” *Clinical Science*, vol. 131, no. 15, pp. 1781–1799, 2017.
 - [43] S. B. Nimse and D. Pal, “Free radicals, natural antioxidants, and their reaction mechanisms,” *RSC Advances*, vol. 5, no. 35, pp. 27986–28006, 2015.
 - [44] S. Heinzelmann and G. Bauer, “Multiple protective functions of catalase against intercellular apoptosis-inducing ROS signaling of human tumor cells,” *Biological Chemistry*, vol. 391, no. 6, pp. 675–693, 2010.
 - [45] G. Bauer, “Autoamplificatory singlet oxygen generation sensitizes tumor cells for intercellular apoptosis-inducing signaling,” *Mechanisms of Ageing and Development*, vol. 172, pp. 59–77, 2018.
 - [46] Marília O. F. Goulart, P. Falkowski, T. Ossowski, and A. Liwo, “Electrochemical study of oxygen interaction with lapachol and its radical anions,” *Bioelectrochemistry*, vol. 59, no. 1–2, pp. 85–87, 2003.
 - [47] N. Watanabe and H. J. Forman, “Autooxidation of extracellular hydroquinones is a causative event for the cytotoxicity of menadione and DMNQ in A549-S cells,” *Archives of Biochemistry and Biophysics*, vol. 411, no. 1, pp. 145–157, 2003.
 - [48] E. T. Sousa, W. A. Lopes, and J. B. Andrade, “Sources, formation, reactivity and determination of quinones in the atmosphere,” *Quimica Nova*, vol. 39, no. 4, pp. 486–495, 2016.
 - [49] L. Galluzzi, I. Vitale, S. A. Aaronson et al., “Molecular definitions of cell death subroutines: recommendations of the Nomenclature Committee on Cell Death 2018,” *Cell Death and Differentiation*, vol. 25, no. 3, pp. 486–541, 2018.
 - [50] Y. T. Su, H. L. Chang, S. K. Shyue, and S. L. Hsu, “Emodin induces apoptosis in human lung adenocarcinoma cells through a reactive oxygen species-dependent mitochondrial

- signaling pathway," *Biochemical Pharmacology*, vol. 70, no. 2, pp. 229–241, 2005.
- [51] W. Lin, M. Zhong, H. Yin et al., "Emodin induces hepatocellular carcinoma cell apoptosis through MAPK and PI3K/AKT signaling pathways in vitro and in vivo," *Oncology Reports*, vol. 36, no. 2, pp. 961–967, 2016.
 - [52] Y. Cui, P. Lu, G. Song, Q. Liu, D. Zhu, and X. Liu, "Involvement of PI3K/Akt, ERK and p38 signaling pathways in emodin mediated extrinsic and intrinsic human hepatoblastoma cell apoptosis," *Food and Chemical Toxicology*, vol. 92, pp. 26–37, 2016.
 - [53] I. Wijesekara, C. Zhang, Q. van Ta, T. S. Vo, Y. X. Li, and S. K. Kim, "Physcion from marine-derived fungus *Microsporium* sp. induces apoptosis in human cervical carcinoma HeLa cells," *Microbiological Research*, vol. 169, no. 4, pp. 255–261, 2014.
 - [54] Y. Han, X. H. Chen, H. Gao, J. L. Ye, and C. B. Wang, "Physcion inhibits the metastatic potential of human colorectal cancer SW620 cells *in vitro* by suppressing the transcription factor SOX2," *Acta Pharmacologica Sinica*, vol. 37, no. 2, pp. 264–275, 2016.
 - [55] J. Y. Hong, H. J. Chung, S. Y. Bae, T. N. Trung, K. H. Bae, and S. K. Lee, "Induction of cell cycle arrest and apoptosis by physcion, an anthraquinone isolated from rhubarb (rhizomes of *Rheum tanguticum*), in MDA-MB-231 human breast cancer cells," *Journal of Cancer Prevention*, vol. 19, no. 4, pp. 273–278, 2014.
 - [56] Q. Wang, Y. Wang, Y. Xing et al., "Physcion 8-O- β -glucopyranoside induces apoptosis, suppresses invasion and inhibits epithelial to mesenchymal transition of hepatocellular carcinoma HepG2 cells," *Biomedicine & Pharmacotherapy*, vol. 83, pp. 372–380, 2016.
 - [57] D. Zhang, Y. Han, and L. Xu, "Upregulation of miR-124 by physcion 8-O- β -glucopyranoside inhibits proliferation and invasion of malignant melanoma cells via repressing RLIP76," *Biomedicine & Pharmacotherapy*, vol. 84, pp. 166–176, 2016.
 - [58] Q. C. Xie and Y. P. Yang, "Anti-proliferative of physcion 8-O- β -glucopyranoside isolated from *Rumex japonicus* Hoult. On A549 cell lines via inducing apoptosis and cell cycle arrest," *BMC Complementary and Alternative Medicine*, vol. 14, no. 1, p. 337, 2014.
 - [59] R. K. Khurana, A. Jain, A. Jain, T. Sharma, B. Singh, and P. Kesharwani, "Administration of antioxidants in cancer: debate of the decade," *Drug Discovery Today*, vol. 23, no. 4, pp. 763–770, 2018.
 - [60] C. Holze, C. Michaudel, C. Mackowiak et al., "Oxeiptosis, a ROS-induced caspase-independent apoptosis-like cell-death pathway," *Nature Immunology*, vol. 19, no. 2, pp. 130–140, 2018.
 - [61] G. Bauer, "HOCl and the control of oncogenesis," *Journal of Inorganic Biochemistry*, vol. 179, pp. 10–23, 2018.
 - [62] T. A. Lehman, R. Modali, P. Boukamp et al., "p53 Mutations in human immortalized epithelial cell lines," *Carcinogenesis*, vol. 14, no. 5, pp. 833–839, 1993.
 - [63] M. Baritaud, H. Boujrad, H. K. Lorenzo, S. Krantic, and S. A. Susin, "Histone H2AX: the missing link in AIF-mediated caspase-independent programmed necrosis," *Cell Cycle*, vol. 9, no. 16, pp. 3186–3193, 2010.
 - [64] C. Éthier, M. Tardif, L. Arul, and G. G. Poirier, "PARP-1 modulation of mTOR signaling in response to a DNA alkylating agent," *PLoS One*, vol. 7, no. 10, article e47978, 2012.
 - [65] M. Shimobayashi and M. N. Hall, "Making new contacts: the mTOR network in metabolism and signalling crosstalk," *Nature Reviews. Molecular Cell Biology*, vol. 15, no. 3, pp. 155–162, 2014.
 - [66] A. Bahrami, M. Hasanzadeh, S. M. Hassanian et al., "The potential value of the PI3K/Akt/mTOR signaling pathway for assessing prognosis in cervical cancer and as a target for therapy," *Journal of Cellular Biochemistry*, vol. 118, no. 12, pp. 4163–4169, 2017.
 - [67] C. Darido, S. R. Georgy, C. Cullinane et al., "Stage-dependent therapeutic efficacy in PI3K/mTOR-driven squamous cell carcinoma of the skin," *Cell Death & Differentiation*, vol. 25, no. 6, pp. 1146–1159, 2018.
 - [68] R. Tamura, K. Yoshihara, T. Saito et al., "Novel therapeutic strategy for cervical cancer harboring *FGFR3-TACC3* fusions," *Oncogene*, vol. 7, no. 1, pp. 4–12, 2018.
 - [69] R. L. B. Costa, H. S. Han, and W. J. Gradishar, "Targeting the PI3K/AKT/mTOR pathway in triple-negative breast cancer: a review," *Breast Cancer Research and Treatment*, vol. 169, no. 3, pp. 397–406, 2018.

